Graduate School ETD Form 9
(Revised 12/07)

PURDUE UNIVERSITY
GRADUATE SCHOOL
Thesis/Dissertation Acceptance

This is to certify that the thesis/dissertation prepared

By Andy Bowei Chen

Entitled
APPLICATION OF QUANTITATIVE ANALYSIS IN TREATMENT OF OSTEOPOROSIS AND OSTEOARTHRITIS

For the degree of Master of Science in Biomedical Engineering

Is approved by the final examining committee:

Hiroki Yokota
Chair

Sungsoo Na

John Schild

To the best of my knowledge and as understood by the student in the *Research Integrity and Copyright Disclaimer (Graduate School Form 20)*, this thesis/dissertation adheres to the provisions of Purdue University's "Policy on Integrity in Research" and the use of copyrighted material.

Approved by Major Professor(s): Hiroki Yokota

Approved by: John Schild 06/06/2013
Head of the Graduate Program Date

APPLICATION OF QUANTITATIVE ANALYSIS IN TREATMENT OF OSTEOPOROSIS AND OSTEOARTHRITIS

A Thesis

Submitted to the Faculty

of

Purdue University

by

Andy Bowei Chen

In Partial Fulfillment of the

Requirements for the Degree

of

Master of Science in Biomedical Engineering

August 2013

Purdue University

Indianapolis, Indiana

ACKNOWLEDGMENTS

First I would like to thank my mentor, Dr. Hiroki Yokota, for his support both in completing this thesis and developing my research skills. His insight and motivation has been invaluable as I slowly grow toward being a competent contributing member of society.

I would also like to thank the other members of my advisory committee, Dr. Sungsoo Na and Dr. John Schild, for their time and advice.

Earnest thanks goes to Dr. Ping Zhang for allowing me to work with him in isolating bone marrow cells from osteoporotic mice and teaching me many techniques. Thanks go to Dr. Kazunori Hamamura for performing siRNA experiments and allowing me to use this data. Thanks go to all my colleagues in Dr. Yokota's lab, including Dr. Simon Shim, Aysan Abedinpoor, Todd Dodge, Enlin Qian, and Nancy Tanjung, for their help and support for this thesis. Special thanks go to Valerie Lim Diemer, for helping me format my thesis, and Shelly Albertson, for helping me with all the administrative work.

Finally, I would like give my warmest thanks to my family, who have supported me throughout my academic career, and my friends, who have kept me sane.

TABLE OF CONTENTS

Page

Page

LIST OF TABLES

LIST OF FIGURES

ABSTRACT

Chen, Andy Bowei. M.S.B.M.E, Purdue University, August 2013. Application of Quantitative Analysis in Treatment of Osteoporosis and Osteoarthritis. Major Professor: Hiroki Yokota.

As our population ages, treating bone and joint ailments is becoming increasingly important. Both osteoporosis, a bone disease characterized by a decreased density of mineral in bone, and osteoarthritis, a joint disease characterized by the degeneration of cartilage on the ends of bones, are major causes of decreased movement ability and increased pain. To combat these diseases, many treatments are offered, including drugs and exercise, and much biomedical research is being conducted. However, how can we get the most out of the research we perform and the treatment we do have? One approach is through computational analysis and mathematical modeling.

In this thesis, quantitative methods of analysis are applied in different ways to two systems: osteoporosis and osteoarthritis. A mouse model simulating osteoporosis is treated with salubrinal and knee loading. The bone and cell data is used to formulate a system of differential equations to model the response of bone to each treatment. Using Particle Swarm Optimization, optimal treatment regimens are found, including a consideration of budgetary constraints. Additionally, an *in vitro* model of osteoarthritis in chondrocytes receives RNA silencing of Lrp5. Microarray analysis of gene expression is used to further elucidate the mode of regulation of ADAMTS5, an aggrecanase associated with cartilage degradation, by Lrp5, including the development of a mathematical model.

The math model of osteoporosis reveals a quick response to salubrinal and a delayed but substantial response to knee loading. Consideration of cost effectiveness showed that as budgetary constraints increased, treatment did not start until later.

The quantitative analysis of ADAMTS5 regulation suggested the involvement of IL1β and p38 MAPK. This research demonstrates the application of quantitative methods to further the usefulness of biomedical and biomolecular research into treatment and signaling pathways. Further work using these techniques can help uncover a bigger picture of osteoarthritis's mode of action and ideal treatment regimens for osteoporosis.

1. INTRODUCTION

1.1 Bone Structure and Remodeling

Bone is the major constituent of the skeletal system. It is responsible for structural support and protection of internal organs, as well as serving as a reservoir for metabolic calcium and phosphate necessary to maintain mineral homeostasis [1]. The inner cavity of bones houses the bone marrow, a tissue responsible for the production of red blood cells through a process called hematopoiesis. Bones are also made up of three major cell types: osteoblasts, osteoclasts, and osteocytes.

Osteoblasts are bone forming cells responsible for producing and depositing bone matrix. They are descendants of multipotent mesenchymal stem cells. Osteoblast progenitors are induced to differentiate by a variety of factors, for example runt-related transcription factor 2 (Runx2) [2] and activating transcription factor 4 (ATF4) [3].

Osteoclasts are bone resorbing cells that degrade bone mineral through acidification and proteolysis. Osteoclasts are giant multinucleated cells descended from hematopoietic stem cells, specifically from macrophages. Osteoclast progenitors differentiate into active osteoclasts by binding macrophage colony-stimulating factor (M-CSF) and receptor activator of nuclear factor κ-B ligand (RANKL). Osteoclasts resorb bone by first binding proteins at the bone surface. Within the bound zone, collagen fibrils are digested and acidified, releasing calcium and phosphate into the cell body [4].

Osteocytes are descendants of osteoblasts trapped in the bone matrix and are responsible for orchestrating much of the bone remodeling activity. Osteocyte processes link to other osteocytes through the canaliculi, forming a bone signaling net-

work. Here, they detect perturbations of the bone and activate the appropriate response [5]. For example, osteocyte expression of sclerostin (Sost), which inhibits osteoblast activity, is reduced by mechanical stimulation *in vivo* [6].

Bone remodeling is a process balancing osteoblast-driven bone formation and osteoclast-driven bone resorption to maintain the bone's mechanical strength and structure. The process is contained in what is termed the basic multicellular unit (BMU) and undergoes five major phases: activation, resorption, reversal, formation, and termination. Bone remodeling is activated after detection of an initiation signal. In resorption, partially differentiated mononuclear pre-osteoclasts migrate to the bone surface and turn into multicellular osteoclasts, which release bone resorbing enzymes. During reversal, the BMU is prepared for subsequent formation by mononuclear cells. Formation occurs once mesenchymal stem cells and osteoblast progenitors enter and begin differentiating and proliferating as mature osteoblasts, that then deposit bone matrix which is then mineralized. Remodeling is terminated when the resorbed bone has been replaced [1, 7].

Much research into treating bone diseases has focused on the regulation of bone remodeling. Several factors have been found to regulate bone remodeling. Parathyroid hormone (PTH) is a regulator of calcium homeostasis that was found to stimulate bone formation when administered intermittently but stimulate bone resorption when administered continuously [8]. Glucocorticoids are anti-inflammatory steroids that also promote apoptosis in osteoblasts and osteoclasts. Excess glucocorticoids can lead to osteonecrosis and osteoporosis [9].

1.2 Osteoporosis

Osteoporosis is a disease that disrupts bone mineral balance in favor of bone resorption, leading to weak, fracture-prone bones of reduced density. One of the most common causes of osteoporosis is menopause in aging women [10]. Menopause is characterized by a gradual decline in ovarian function, leading to decreased estrogen

production. Since estrogen inhibits osteoclast activity, its decrease leads to an increase in bone resorption [11].

To combat this, several treatments are available. Bisphosphonates, such as alendronate, ibandronate, risedronate, and zoledronate, are pyrophosphate analogues that suppress bone resorption by binding to bone mineral and preventing osteoclast attachment to the bone surface [12]. Denosumab is a human antibody to receptor activator of nuclear factor-$\varkappa$B (RANK) ligand (RANKL) that blocks its binding to RANK, a receptor on osteoclasts necessary for osteoclast formation, thereby blocking osteoclast bone resorption [13, 14]. Teriparatide, recombinant human PTH, mimics PTH's bone-forming effects to fight the catabolic effects of osteoporosis [15].

Ovariectomized mice are used as an animal model for postmenopausal osteoporosis [16]. The ovaries are the primary source of estrogen production in females. By surgically removing the ovaries, estrogen production decreases, resulting in a decrease in bone density modeling postmenopausal osteoporosis.

1.3 Knee Loading

Weight-bearing exercise has been demonstrated to counteract some osteoporosis-induced bone loss [17, 18]. Many different loading modalities have been used to promote load-driven bone formation. Knee loading has been shown to lead to bone formation [19]. In this loading method, shown in Figure 1.1, the epiphyses of the proximal tibia and the distal femur are loaded, increasing intramedullary pressure in the adjacent bones. This pressure leads to interstitial fluid flow, which has been shown to induce bone formation [20, 21].

1.4 Salubrinal

Injection of salubrinal, a selective inhibitor of the de-phosphorylation of eukaryotic translation initiation factor 2 alpha (eIF2α) [22], is being investigated as a possible treatment for osteoporosis. Salubrinal treatment stimulates *in vitro* matrix deposition

and expression of activating transcription factor 4 (ATF4) in osteoblasts, critical for osteoblastogenesis [3], while inhibiting protein expression levels of nuclear factor of activated T-cells c1 (NFATc1), important in osteoclastogenesis [23], and reducing differentiation of osteoclasts [24, 25].

1.5 Joint and Cartilage Maintenance

Joints are locations at which two or more bones meet. They are responsible for much of the range of movement of the skeleton. The knee joint in particular is a compound synovial joint consisting of two condylar joints between the tibia and femur and a sellar joint between the femur and patella. The lateral and medial condyles

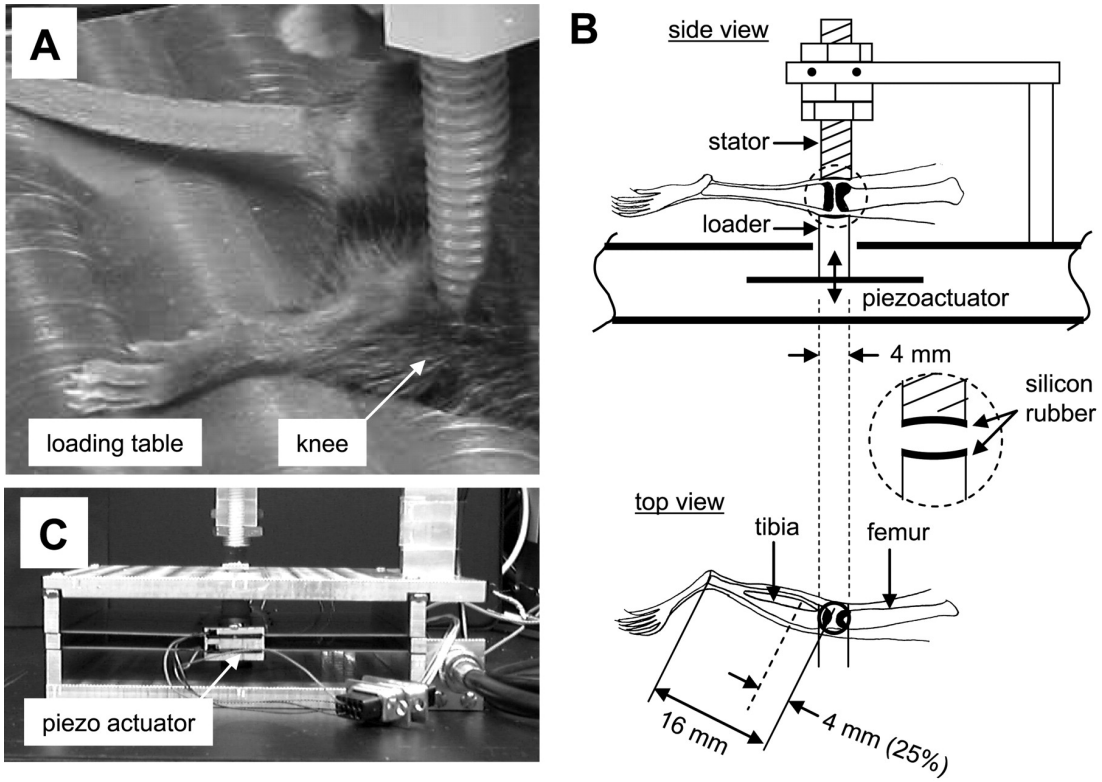

Fig. 1.1. Diagram of knee loading technique. (A) Photograph of knee loading on mouse. (B) Diagram of knee between loader and stator, from the side and top. (C) Photograph of piezo actuator that produces force on the loader. Adapted from [19].

of the tibia and femur bear articular cartilage, and the meniscus, a thick pad of cartilage, separates the two. The anterior and posterior cruciate ligaments (ACL and PCL) serve to stabilize the rotation of the joint [26].

Chondrocytes are the terminally differentiated descendants of the mesenchymal stem cell line and the single cellular component of adult hyaline cartilage that, under normal conditions, maintain the cartilage matrix [27]. Cartilage anabolism is controlled by the expression of several genes in chondrocytes, including type II collagen, Sox-9, and Aggrecan [28]. The extracellular matrix (ECM) of cartilage consists of proteoglycan and hyaluronan complexes embedded in three-dimensional collagen-composed heterotypic fibrils. The ECM is responsible for much of the cartilage characteristics.

1.6 Osteoarthritis and Wnt Signaling

Osteoarthritis (OA) is a prevalent and chronic condition characterized by a progressive breakdown of the joint cartilage between two bones caused by abnormal remodeling by inflammatory factors [29]. Patients with OA often suffer from joint pain, inflammation, and a general decrease in joint function. Severe cases may even require joint replacement. In OA, chondrocyte-matrix association is often disrupted, initially leading to transient proliferation; however, catabolic cytokines are quickly generated, and the cartilage begins to break down. Loss of proteoglycans and type II collagen cleavage result in increased water content that decreases tensile strength [27].

Matrix metalloproteinases (MMPs) are well-established proteins that degrade collagens and proteoglycans in OA. Of this family, MMP-1, -2, -3, -8, -9, -10, -11, -13, and -14 have been implicated as major catabolic players in OA. The a disintegrin and metalloproteinase with thrombospondin motifs (ADAMTS) family of aggrecanases has recently been a target of OA study for their proteoglycan degrading properties [30]. Specifically, ADAMTS4 and ADAMTS5 have been investigated as the major aggrecanases of OA. Aggrecan has the ability to form multimolecular aggregates.

Its hydrophilic properties improve the compression and shear resistance of cartilage and tendon [30]. Aggrecanases work to disrupt this function, degrading the cartilage matrix, leading to articular cartilage degradation.

Some evidence suggests that the Wnt signaling pathway is involved in the mechanism of osteoarthritis [31]. Wnt3A treatment and forced expression of β-catenin in rabbit articular chondrocyte cultures stimulated gelatinase activity and expression of MMP3 and MMP13, as well as ADAMTS4 and ADAMTS5 [32]. Mice induced with loss of FRZB, an antagonist of the Wnt pathway, after induction of OA, exhibited greater cartilage loss than wild type, suggesting that Wnt signaling increases cartilage degradation in OA [33].

Low-density lipoprotein receptor-related protein 5 (LRP5), a transmembrane protein that acts as a co-receptor for Wnt signaling proteins, is known to be a key regulator of bone formation. Lrp5-knockout mice have deficient bone mass and strength [34]. Its role in OA is less understood. Lrp5-knockout mice exhibit increased cartilage degradation when OA is induced, suggesting that Lrp5 is necessary to prevent cartilage degradation in OA [35]. However, a separate study found that β-catenin and Lrp5 expression was increased in osteoarthritic chondrocytes, and silencing Lrp5 by siRNA in osteoarthritic chondrocytes downregulated the expression of MMP13, suggesting that Lrp5 stimulates cartilage degradation [36].

1.7 Metaheuristic Optimization Algorithms

Metaheuristics are optimization procedures that sacrifice optimality for speed in order to find near-optimal solutions to large complex problems [37]. They are often helpful to find solutions to problems with a large set of potential solutions. Two such algorithms are Particle Swarm Optimization (PSO) and Ant Colony Optimization (ACO). Particle Swarm Optimization simulates the behavior of a swarm of particles searching for a best solution, mimicking the social behavior of organisms such as birds, fish, or bees. In PSO, each particle uses its knowledge of its own historical

best position and the knowledge of the entire swarm's historical best position to move toward an optimum position [38]. For example, in Figure 1.2, Particles 1 and 2 are shown. Each particle is attempting to find the best solution in the solution space. After every time step, each particle assesses its next move by considering the best solution its had as well as the best solution in the entire swarm. Eventually, a near-optimal solution will be settled on.

Ant Colony Optimization mimics the behavior of ant colonies in finding sources of food, as illustrated in Figure 1.3. At first, ants leave the colony and randomly search for food. When they find a food source, they retrace their steps back to the ant colony, depositing pheromones along the way. Other ants will follow these pheromones and, upon finding food, reinforce the trails. Since the pheromones evaporate, shorter paths will be more frequently reinforced and thus have stronger pheromone concentrations, until the near-optimal path (solution) is found [40].

In this thesis, PSO and ACO will be implemented for two separate purposes. PSO will be utilized for optimizing treatment regimens, because we are looking for a single

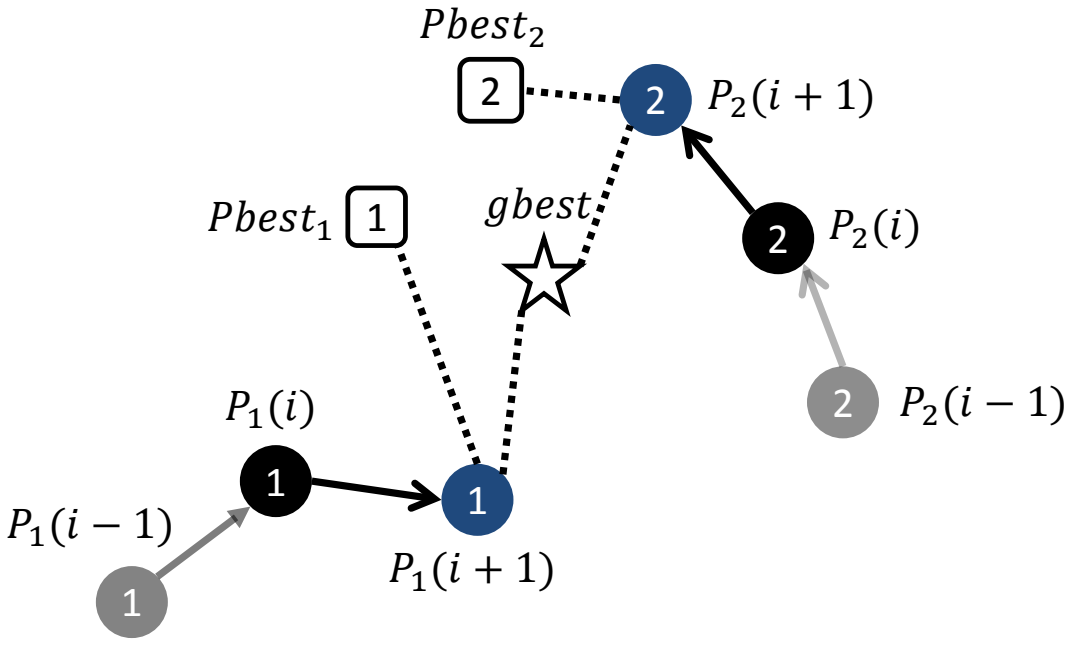

Fig. 1.2. Illustration of Particle Swarm Optimization

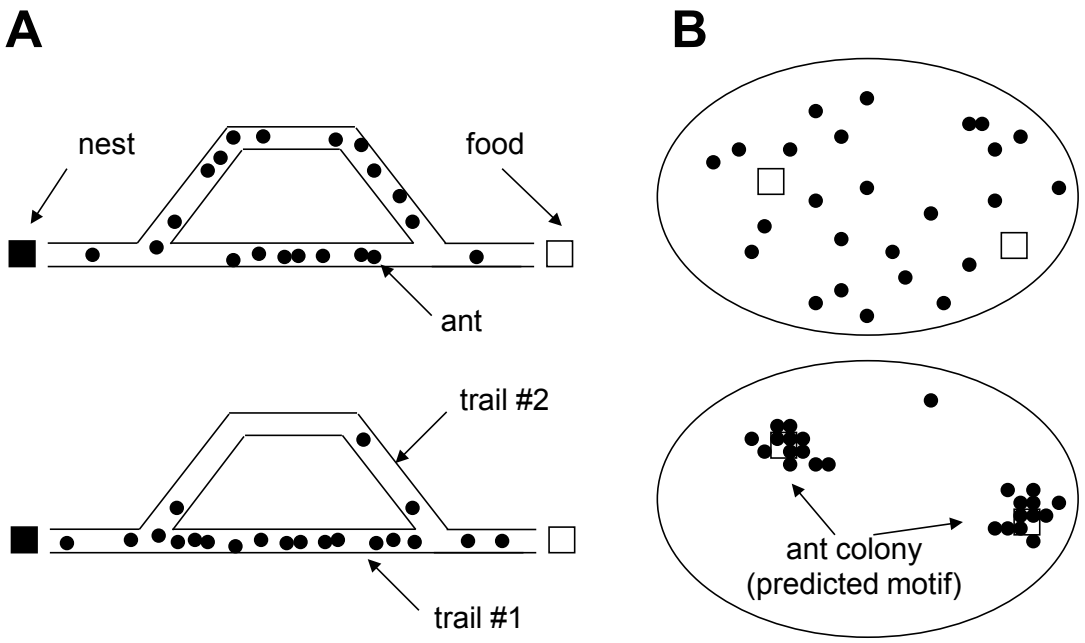

Fig. 1.3. Illustration of Ant Colony Optimization, adapted from [39].

optimal solution. The PSO will be implemented with an exit criteria instead of a fixed iteration number, which makes the solution time more variable but decreases excessive computation after an optimal solution is found. ACO will be utilized to look for potential transcription factor binding motifs (TFBMs), short sequences in the promoter region of a gene that are a part of the sequence that transcription factors bind to. For this, we are not necessarily looking for an optimal combination of TFBMs, but rather we want ideas about which TFBMs are important indicators of gene expression from experimental conditions.

1.8 Problem Statement

Osteoporosis and osteoarthritis are well-studied diseases, but there is still room to improve treatment outcomes. New treatments are being researched constantly. *In vivo* and *in vitro* experiments have been used for decades to try to understand the

molecular pathways involved in bone and joint maintenance. However, the usefulness of these data can be extended using mathematical modeling techniques.

1.9 Objectives

This thesis aims to apply mathematical concepts to *in vivo* and *in vitro* experimental data to improve our understanding of pathways and help improve treatment outcomes. This will be accomplished in two ways: first, a mouse model of osteoporosis will be mathematically modeled along with different treatments in order to find the optimal treatment regimen; second, a series of RNA silencing experiments on chondrocytes will be used to help create a model of Lrp5's involvement in osteoarthritis.

2. METHODS

2.1 Osteoporosis Animal Study

C57BL/6 female mice (8 weeks old) were housed four to five mice per cage at the Indiana University Animal Care Facility and fed with mouse chow and water *ad libitum*. All experimental procedures were approved by the Indiana University School of Medicine Institutional Animal Care and Use Committee to be compliant with the Guiding Principles in the Care and Use of Animals endorsed by the American Physiological Society. A timeline of the animal experiments is shown in Figure 2.1.

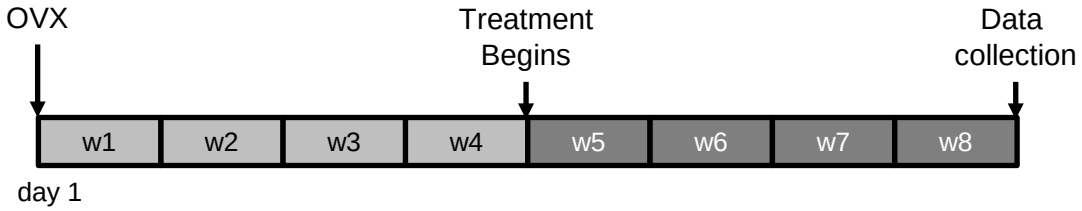

Fig. 2.1. Timeline of the experimental protocol

2.1.1 Ovariectomy

Animals were anesthetized using 1.5% isoflurane at flow rate 0.5-1.0 L/min. The operation site was shaved and cleaned with 70% alcohol and 10% povidone-iodine solution. An approximately 20 mm incision was cut at the midline dorsal skin, and the peritoneal cavity was incised to access and remove the ovaries. The wound was closed by suture, and the mice were given 4 weeks to recover before treatment began.

2.1.2 Knee Loading

Each mouse was anesthetized in an anesthetic induction chamber using isoflurane. Each anesthetized mouse was then placed on a custom-made piezoelectric loading platform where they continued to be mask-anesthetized with 2% isoflurane. Loads were applied in the lateral-medial direction for 3 minutes/day at 15Hz, with peak-to-peak force of 0.5 N. These conditions were chosen based on previous studies [19]. For the sham-loading control, each mouse was prepared in the same way, but the voltage signal was not applied.

2.1.3 Salubrinal Administration

Twenty-four mice were injected subcutaneously with salubrinal (Tocris Bioscience, Ellisville, MO, USA) solution dissolved in dimethyl sulfoxide (DMSO) (1 mg/kg body weight) daily for 4 weeks. The control group (another 24 mice) was subcutaneously injected with a vehicle control consisting of only solvent DMSO.

2.1.4 Data Collection

The bone mineral density of the femur was determined with peripheral dual energy X-ray absorptiometry (DXA; PIXImus II; Lunar Corp., Madison, WI, USA) and the Lunar Piximus software (version 1.47).

Bone marrow-derived cells were collected from sacrificed mice by flushing the iliac, femur, and tibia with Iscove's MEM (Gibco-Invitrogen, Carlsbad, CA, USA) supplemented with 2% fetal bovine serum using a 23-gauge needle. Low-density gradient centrifugation was performed to separate the cells. The cells were then plated on 6-well plates at cell density 2×10^6 cells/mL in osteogenic differentiation medium (MesenCult proliferation kit) supplemented with 10 nM dexamethasone, 50 µg/mL ascorbic acid 2-phosphate, and 10 mM β-glycerophosphate to induce osteogenic differentiation. The medium was changed every other day. After two weeks, the cells were fixed with citrate-buffered acetone (30 sec), incubated in alkaline-dye mix (30

min), and then counterstained with Mayer's Hematoxylin (10 min). The number of ALP stained and unstained colonies were counted to determine osteoblast activity.

Bone marrow-derived cells were applied to 96-well plates in α-MEM supplemented with 10% FBS, 30 ng/ml M-CSF, and 20 ng/ml murine receptor activator of nuclear factor κ-B ligand (RANKL). On day 4, the medium was changed. On day 6, the adherent cells were fixed and stained using a tartrate resistant acid phosphate (TRACP) staining kit. TRACP-positive multinucleated cells (more than 3 nuclei) were identified, and the osteoclast coverage area was determined.

2.2 Osteoarthritis *In vitro* Study

2.2.1 Cell Culture

C28/I2 human chondrocytes were cultured in DMEM containing 10% fetal bovine serum and antibiotics (50 units/ml penicillin and 50 µg/ml streptomycin; Life Technologies, Grand Island, NY, USA). Cells were maintained at 37℃ and 5% CO_2 in a humidified incubator. 1 ng/ml IL1β (R&D Systems, Minneapolis, MN, USA) stimulation was performed after 10 h in serum-free conditions.

2.2.2 RNA Interference with siRNA

Cells were treated with siRNA specific to Lrp5, IL1β (Life Technologies) and p38 MAPK (Cell Signaling, Danvers, MA, USA). The selected target sequences for knockdown of Lrp5a, Lrp5b, p38 MAPK, and IL1β were: Lrp5a, 5'-GUACAGGCCC UACAUCAUU-3'; Lrp5b, 5'-CGUUCGGUCUGACGCAGUA-3'; p38 MAPK, 5'- G CCCAUAAGGCCAGAAACU -3'; and IL1β, 5'-CGAUGCACCUGUACGAUCA-3'. Note that Lrp5a siRNA and Lrp5b siRNA are two independent siRNAs specific to Lrp5. As a nonspecific control, negative siRNA (Silencer Select #1, Life Technologies and SignalSilence Control siRNA, Cell Signaling) were used. Cells were transiently

transfected with siRNA in Opti-MEM I medium with Lipofectamine RNAiMAX (Life Technologies). Six hours later, the medium was replaced by regular culture medium. The efficiency of silencing was assessed with immunoblotting and quantitative real-time PCR at 48 h after transfection.

2.2.3 Quantitative Real-time PCR

Total RNA was extracted using an RNeasy Plus mini kit (Qiagen, Germantown, MD, USA). Reverse transcription was conducted with high capacity cDNA reverse transcription kits (Applied Biosystems, Carlsbad, CA, USA), and quantitative real-time PCR was performed using ABI 7500 with Power SYBR green PCR master mix kits (Applied Biosystems). We evaluated mRNA levels of ADAMTS5, IL1β, IL6, IL8, IL12A, IL15, IL16, and IL18 with the PCR primers listed in Table 2.1. GAPDH was used for internal control, and the relative mRNA abundance for the selected genes was obtained with respect to the level of GAPDH mRNA.

Table 2.1
Real-time PCR primers used

Gene	Forward Primer	Reverse Primer
ADAMTS5	5'- CACTGTGGCTCACGAAATCG -3'	5'- CGCTTATCTTCTGTGGAACCAAA -3'
IL1	5'- GCTGAGGAAGATGCTGGTTC -3'	5'- TCCATATCCTGTCCCTGGAG -3'
IL6	5'- TACCCCCAGGAGAAGATTCC -3'	5'- TTTTCTGCCAGTGCCTCTTT -3'
IL8	5'- GTGCAGTTTTGCCAAGGAGT -3'	5'- ACTTCTCCACAACCCTCTGC -3'
IL12A	5'- GATGGCCCTGTGCCTTAGTA -3'	5'- TCAAGGGAGGATTTTTGTGG -3'
IL15	5'- AGCTGGCATTCATGTCTTCA -3'	5'- TGGGGTGAACATCACTTCC -3'
IL16	5'- CACGGTGACACTGGAGAAGA -3'	5'- TGATGATGTTCCAGGCTTCA -3'
IL18	5'- GCATCAACTTTGTGGCAATG -3'	5'- ATAGAGGCCGATTTCCTTGG -3'
GAPDH	5'- GCACCGTCAAGGCTGAGAAC -3'	5'- ATGGTGGTGAAGACGCCAGT -3'

2.2.4 Western Immunoblotting

Cells were lysed in a radioimmunoprecipitation assay (RIPA) buffer containing protease inhibitors (Santa Cruz Biotechnology, Santa Cruz, CA, USA) and phosphatase inhibitors (Calbiochem, Billerica, MA, USA). Isolated proteins were fractionated using 10% SDS gels and electro-transferred to Immobilon-P membranes (Millipore, Billerica, MA, USA). The membrane was incubated for 1 h with primary antibodies followed by 45 min incubation with goat anti-rabbit or anti-mouse IgG conjugated with horseradish peroxidase (Cell Signaling). We used antibodies against p38 MAPK, p-p38 MAPK, Lrp5 (Cell Signaling), and β-actin (Sigma). Protein levels were assayed using SuperSignal West Femto maximum sensitivity substrate (Thermo Scientific), and signal intensities were quantified with a luminescent image analyzer (LAS-3000, Fuji Film, Tokyo, Japan).

2.2.5 Gene Expression Microarray

Microarray experiments were conducted using Agilent Whole Human Genome arrays (Human 8 × 60K array, Agilent). Eight RNA samples isolated from 4 pairs of C28/I2 chondrocyte cells (transfected with control and Lrp5a siRNAs) were labeled with the Agilent low RNA input fluorescent linear amplification kit. They were hybridized to 8 one-color arrays using the in situ hybridization kit (Agilent). Microarray data were filtered to remove background noise and a modified t-test was performed to identify a group of genes that were altered greater than 2-fold or less than 0.5-fold with statistical significance at $p < 0.01$.

2.3 Computational Analysis

2.3.1 Osteoporosis Treatment Modeling

2.3.1.1 Model Definition

In addition to the OPG/RANK/RANKL pathway interaction with osteoblasts and osteoclasts defined previously [41], four molecular players, estrogen, sclerostin, ATF4, and NFATc1, were included with BMD in an expanded mathematical model of bone remodeling (Figure 2.2). Three experimental conditions were also modeled. OVX was modeled to reduce bone mineral density (BMD) via estrogen, while knee loading and salubrinal application elevated BMD via sclerostin and phosphorylated eIF2α (p-eIF2α), respectively. NFATc1 was added as a p-eIF2α-dependent intermediary between RANK-RANKL and osteoclast precursor synthesis. ATF4 was included as a p-eIF2α-dependent promoter of osteoblast differentiation. The associated equations can be found in Appendix A. The state variables and their reference values are summarized in Table 2.2.

2.3.1.2 Optimizing the Model Solver

The system of differential equations was initially solved in MATLAB (version 2011b; MathWorks) using the solver function *ode45*. To improve calculation speed without sacrificing solution accuracy, each of the seven types of solvers in MATLAB. For *ode23s*, *ode23tb*, and *ode15s*, two additional conditions were used setting the maximum iteration step size ('MaxStep') at 0.5 and 0.1. In all, 13 solver cases were tried and applied to 20 randomly generated 8-week treatment regimens. Each solving condition's accuracy was characterized by comparing it to the solution using the *ode45* solver. Solver goodness was judged by balancing the solving time with solution ac-

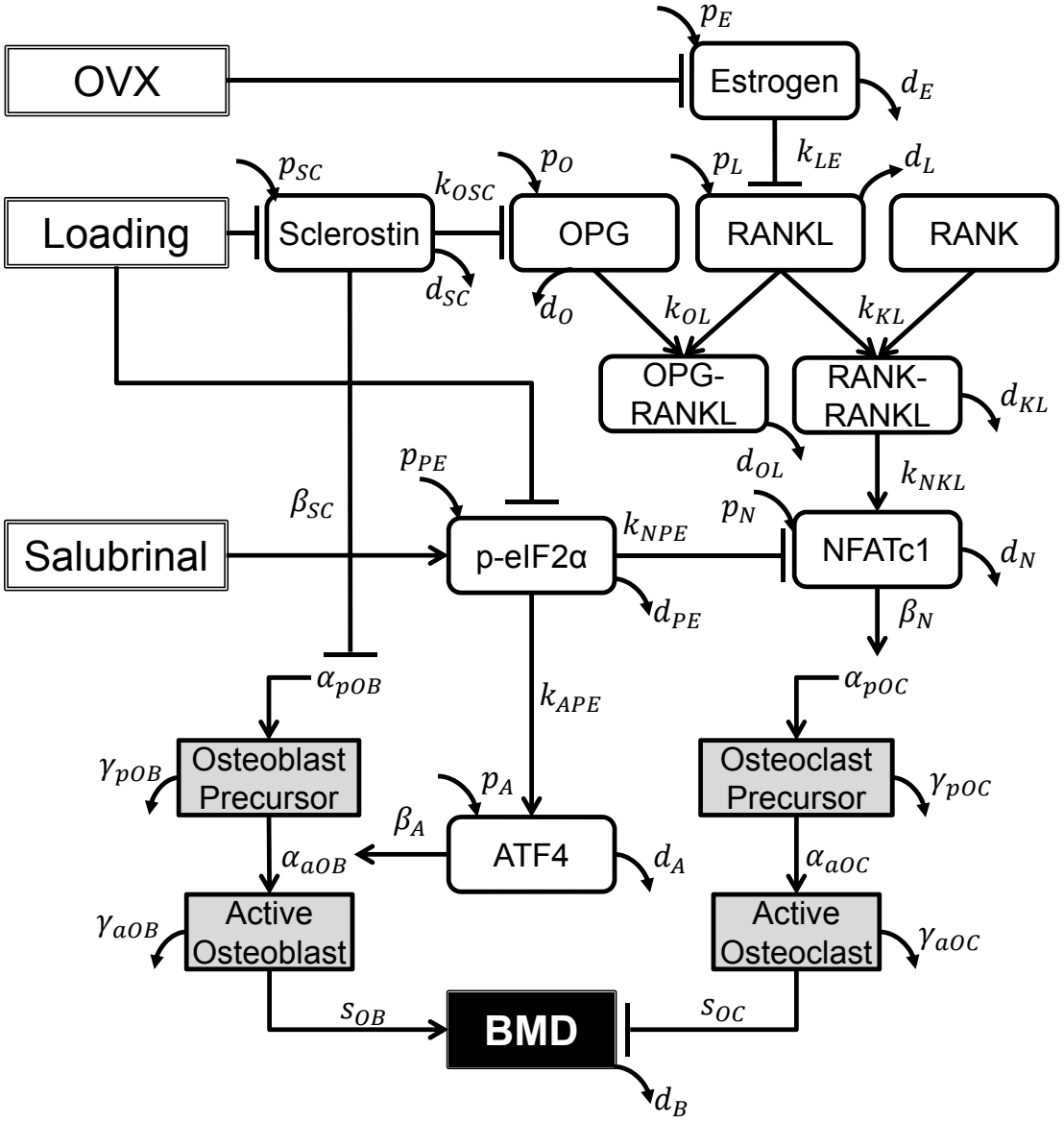

Fig. 2.2. A networked schematic detailing the molecular and cellular interactions of the model. Ovariectomy (OVX) is modeled to reduce bone mineral density (BMD) via estrogen, while knee loading and salubrinal application elevate BMD via sclerostin and phosphorylated eIF2α, respectively. OPG: osteoprotegerin; RANK: receptor activator of nuclear factor kappa-B; RANKL: RANK ligand; p-eIF2α: phosphorylated eukaryotic translation initiation factor 2α; NFATc1: nuclear factor of activated T-cells, cytoplasmic 1; and ATF4: activating transcription factor 4.

Table 2.2
State variables and initial values

State Variable	Description	Reference Value
x_O	OPG	5.5×10^2 nM
x_L	RANKL	15.9×10^0 nM
x_{OL}	OPG-RANKL	8.75×10^2 nM
x_{KL}	RANK-RANKL	4.77×10^2 nM
N_{pOB}	Precursor Osteoblasts	3200
N_{aOB}	Active Osteoblasts	19
N_{pOC}	Precursor Osteoclasts	13.8
N_{aOC}	Active Osteoclasts	1.38
B	Bone Mineral Density	0.315 g/cm^3
x_{SC}	Sclerostin	1.5×10^{-1} nM
x_E	Estrogen	1×10^0 nM
x_{PE}	Phosphorylated eif2α	1×10^{-1} nM
x_A	ATF4	2×10^{-1} nM
x_N	NFATc1	6.27×10^{-2} nM

curacy. Solution accuracy was defined as the difference from *ode45* of the final BMD value.

To model the experimental conditions, salubrinal and loading treatments were applied during weeks 5-8 under normal and ovariectomized conditions, and the final BMD, osteoblast, and osteoclast numbers were compared to the experimental results.

2.3.1.3 Parameter Adjustment and Sensitivity

Initial values of the state variables and parameters were approximated to analogous variables and parameters in the previous model [41]. For new variables and parameters, existing literature was consulted to use biologically relevant magnitudes, but

most were approximations. After setting initial magnitudes, parameters were adjusted to approximate the results of the *in vivo* ovariectomy experiments under each treatment compared to the untreated ovariectomy state.

To help identify which parameters to vary and by how much, the sensitivity of several parameters were determined. These parameters were varied from 1/100 to 100 times their initial value, and the peak changes in BMD and osteoclast or osteoblast were determined. In each case, salubrinal or loading treatment was applied during weeks 5-8 to the OVX condition and compared to the sham treatment case. For the osteoclast-related parameters (k_{OL}, d_{OL}, k_{KL}, and d_{KL}), the largest increases in BMD from treatment and the largest decreases in active osteoclasts were calculated. Osteoblast-related parameters (β_A, β_{SC}, and k_{APE}) were varied under treatment to find the largest increases in BMD and active osteoblast number.

Using this information, the values of parameters were adjusted so that the model simulation approximated the experimental results. Additionally, variable magnitudes and long-term dynamics were kept realistic. The parameters and their default values are summarized in Table 2.3.

Table 2.3: Parameter definitions and values

Parameter	Description	Value
p_O	Production of OPG	200 nM/day
d_O	Degradation of OPG	0.2 1/day
p_L	Production of RANKL	70 nM/day
d_L	Degradation of RANKL	2.2 1/day
k_{OL}	OPG-RANKL Complex Rate	1 1/(nM day)
d_{OL}	OPG-RANKL Dissociation Rate	10 1/day
k_{KL}	RANK-RANKL Complex Rate	6 1/(nM day)
d_{KL}	RANK-RANKL Dissociation Rate	0.2 1/day
α_{pOB}	Synthesis of Precursor Osteoblasts	80 1/day

Table 2.3: continued

γ_{pOB}	Degradation of Precursor Osteoblasts	0.01 1/day
α_{aOB}	Synthesis of Active Osteoblasts	0.01 1/day
γ_{aOB}	Degradation of Active Osteoblasts	2 1/day
α_{pOC}	Synthesis of Precursor Osteoclasts	1 1/day
γ_{pOC}	Degradation of Precursor Osteoclasts	0.1 1/day
α_{aOC}	Synthesis of Active Osteoclasts	0.2 1/day
γ_{aOC}	Degradation of Active Osteoclasts	2 1/day
β_A	ATF4 Interaction with Osteoblasts	0.01 1/(nM day)
β_N	NFATc1 Interaction with Osteoclasts	50 1/(nM day)
β_{SC}	Sclerostin Interaction with Osteoblasts	65 1/(nM day)
p_{SC}	Production of Sclerostin	3 nM/day
d_{SC}	Degradation of Sclerostin	20 1/day
p_E	Production of Estrogen	1 nM/day
d_E	Degradation of Estrogen	1 1/day
k_{LE}	Interaction of Estrogen with RANKL	35 1/day
p_{PE}	Production of P-eif2α	0.1 nM/day
d_{PE}	Degradation of P-eif2α	1 1/day
p_A	Production of ATF4	0.01 nM/day
d_A	Degradation of ATF4	0.1 1/day
p_N	Production of NFATc1	3 nM/day
d_N	Degradation of NFATc	100 1/day
k_{NKL}	Interaction of RANK-RANKL with NFATc1	0.01 1/day
k_{OSC}	Interaction of Sclerostin with OPG	600 1/day
k_{APE}	Interaction of P-eif2α with ATF4	0.1 1/day
k_{NPE}	Interaction of P-eif2α with NFATc1	15 1/day
x_K	RANK	1 nM

2.3.1.4 Treatment Selection

The selection problem in this study was to determine the sequence of three weekly treatment options (no treatment, knee loading, or salubrinal) over 8 and 16 weeks which maximally suppressed the decrease of BMD in ovariectomized mice. The optimal sequence was obtained for 8-week treatment by a brute force search of all possible combinations, while a heuristic search algorithm, particle swarm optimization, was used to find near-optimal treatment regimens for 16-week treatment.

2.3.1.5 Particle Swarm Algorithm

The particle swarm algorithm in this study was based on our previous implementation for predicting transcription factor binding motifs [42]. Each particle contained a probability vector for each treatment for each week. During every run, particle candidates were created by using those probabilities, and the velocities calculated updated the probabilities. The velocity was calculated:

$$V_i(t) = V_i(t-1) + \alpha\Big(\lambda_g\big(P_{gbest}(t-1) - P_i(t-1)\big) + \beta\lambda_{Pi}\big(P_{pbest(i)}(t-1) - P_i(t-1)\big)\Big) \quad (2.1)$$

where V_i is the velocity of the i-th particle, α is the velocity correction factor, β is the global contribution ratio, P_{gbest} is the global optimal solution, $P_{pbest(i)}$ is the i-th particle's local best, P_i is the current solution of the i-th particle, and λ_g and $\lambda_P i$ are random numbers from 0 and 1. Thus the particle's new position was determined:

$$P_i(t+1) = P_i(t) + V_i(t) \quad (2.2)$$

The particle's fitness was determined by the increase in BMD over the baseline OVX condition at the end of the treatment period. The computation continued until the global best solution was not improved upon for 5 iterations.

To examine the algorithm's parameter sensitivity, the velocity correction factor α and global contribution ratio β were varied and the global best was recorded after

each iteration. Each parameter combination was performed 10 times in an attempt to optimize an 8-week training regimen.

2.3.1.6 Treatment Costs

The fitness function was modified to include a unit cost for each type of treatment such that:

$$J = (\Delta B)^2 - k_{cost}(\epsilon N_{sal} + N_{load})^2 \tag{2.3}$$

where J is the function to minimize, ΔB is the change in the final BMD from the initial BMD, k_{cost} is the treatment cost contribution, ϵ is the cost ratio of salubrinal to knee loading, N_{sal} is the number of salubrinal injections, and N_{load} is the number of loading bouts.

2.3.2 Osteoarthritis Pathway Analysis

2.3.2.1 Transcription Factor Binding Motif Prediction

Using an ant algorithm–based prediction method, potential transcription factor binding motifs were found. In brief, the ant algorithm is a metaheuristic optimization technique based on the biological behavior of ant colonies [43]. Ants initially wander randomly until they find a food source. When they do, they return to the colony, depositing pheromones along the way. Other ants find and follow these pheromones so that shorter routes to better food sources will be reinforced. In our application, paths were sets of 20 6-basepair motifs. Each candidate motif consists of itself and its reverse complement, since transcription factors are assumed to be direction-agnostic. Pheromone levels were found by finding the error between the actual gene expression

levels and the predicted expression levels from the contributions of the chosen motifs. The predicted expression level was defined as:

$$\hat{Z}_n = H_{n\times m}\left(\left(H_{n\times m}^T H_{n\times m}\right)^{-1} H_{n\times m}^T Z_n\right) \tag{2.4}$$

where n is the gene, m is the motif, $\hat{Z}_n$ is the predicted gene expression, Z_n is the actual gene expression, and h_{ij} in $H_{n\times m}$ is the number of j-th occurring in the i-th gene's promoter region (defined as the 1,000-bp region upstream of the gene start site). The cost function was defined as the squared difference between the predicted expression and the actual expression level:

$$C_n = \left(\frac{1}{(Z_n - \hat{Z}_n)^2}\right)^{\alpha} \tag{2.5}$$

where $\alpha > 1$ is the pheromone deposition power. The pheromone level p of motif j after iteration $i+1$ was updated as follows:

$$p_{j,i+1} = p_{j,i}(1-\epsilon) + \frac{1}{C_n(j)} \tag{2.6}$$

where ϵ is the pheromone evaporation rate, and $C_n(j)$ is the sum of the cost functions of motif j. After each iteration, the pheromone levels were updated, and the next TFBMs were chosen based on the current pheromone levels, with motifs with higher pheromone levels more likely to be chosen.

At the end of the analysis, the TFBMs with the highest pheromone levels were further analyzed using the TRANSFAC 7.0 Public 2005 database [44] by searching promoter sites containing the predicted motif sequences. Human genes were chosen for further analysis via literature search, and potentially important pathways were identified. These molecules were submitted to further experiments using RNA silencing, including double silencing combinations.

2.3.2.2 Regulatory Pathway Model

A linear model of the pathway involving Lrp5, p38, IL1β, and ADAMTS5 was built using data from siRNA-knockout experiments. The model consisted of three state

variables, x_1 (LRP5), x_2 (IL1β), and x_3 (p-p38), and one measurement variable, y (ADAMTS5 mRNA level):

$$\Delta y = -\tilde{c}x_1 + f\tilde{x}_2 + d\tilde{x}_3 + h \tag{2.7}$$

$$\tilde{c} = c + e\tilde{x}_2 \tag{2.8}$$

$$\tilde{x}_2 = x_2 - ax_1 \tag{2.9}$$

$$\tilde{x}_3 = x_3 - bx_1 + g\tilde{x}_2 \tag{2.10}$$

where $\tilde{x}_i$ represented the apparent contribution of x_i. Parameters a, b, and c linked the effects of Lrp5 to the three state variables, while parameters d to g governed the other interactions in the pathway, with parameter h representing all interactions not affected by Lrp5. The final form of the measurement variable was expressed:

$$\Delta y = (-c - af - db - adg)x_1 + (f + dg)x_2 + dx_3 - ex_1x_2 + aex_1^2 + h \tag{2.11}$$

$$y = y_0 + \Delta y \tag{2.12}$$

where y_0 is the basal level of ADAMTS5, set to 1. The parameters were solved algebraically based on experimental data.

2.4 Statistical Analysis

Mean and standard deviation was calculated, and a one-way analysis of variance (ANOVA) was performed to test for significance among groups. To find significant differences between different groups, *post hoc* tests were conducted, such as Tukey's test and Bonferroni correction.

3. RESULTS

3.1 Osteoporosis Model

To build the math model of bone remodeling, experimental data was first collected to examine the effects of ovariectomy, knee loading, and salubrinal treatment on the osteoblast activity, osteoclast activity, and bone mineral density of mice. These results, along with a literature survey of relevant molecules and pathways involved in bone remodeling, allowed us to build upon our previously defined model of bone remodeling. The solving conditions were studied so that solutions were accurate and performed in a reasonable time period. Using parameter sensitivity analysis, the parameters were tweaked so that the model solution reflected the results obtained from experiment. Particle Swarm Optimization was then applied to find the optimal treatment regimens. The fitness of the optimization was altered so that restrictions of budget were accounted for, and those associated parameters were analyzed.

3.1.1 Effect of Salubrinal and Loading

The effect of salubrinal and loading treatment on ovariectomized mice is shown in Figure 3.1. After 8 weeks, the BMD of ovariectomized mice decreased by 22%. The 39% increase in osteoclast area accounts for this change. Under 4-week salubrinal application, the BMD of ovariectomized mice decreased only 13%, with osteoblast activity increasing 136% while osteoclast activity decreased by 48%. After 4 weeks of knee loading, the BMD of ovariectomized mice decreased only 12%, with osteoblast activity increasing 136% osteoclast decreasing 34%.

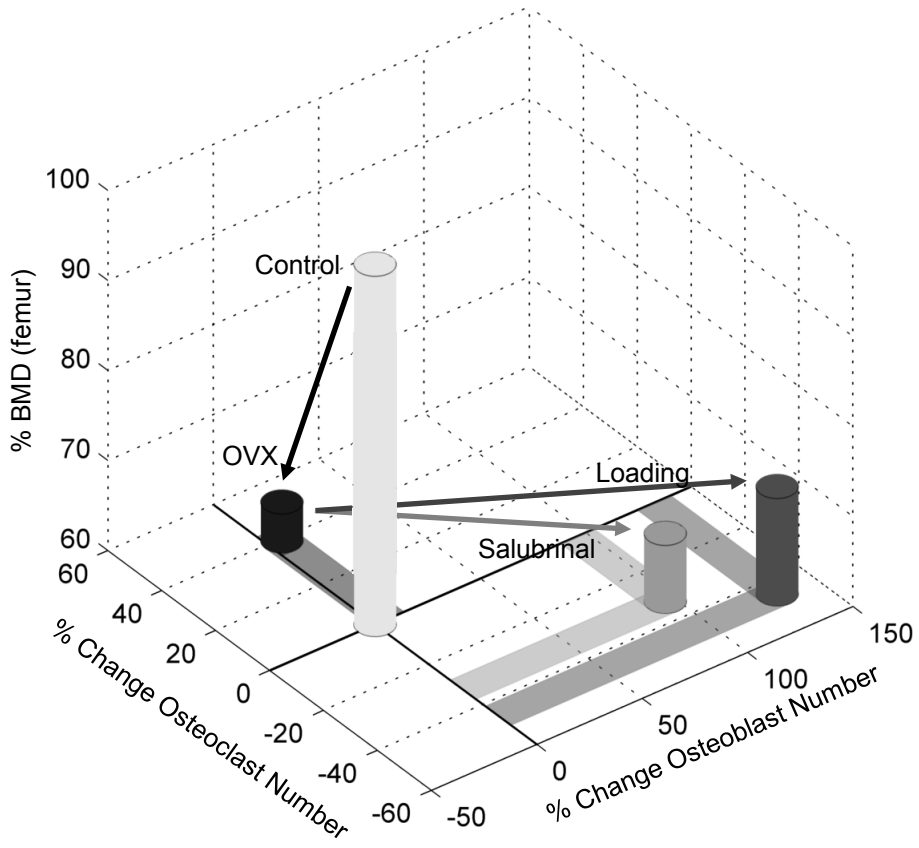

Fig. 3.1. Normalized results of ovariectomy and subsequent loading and salubrinal on BMD, osteoblast, and osteoclast numbers.

3.1.2 Choosing Solver Conditions

The possible solver conditions and their solution times and errors are shown in Table 3.1. *Ode45* was treated as the best solution, and the solution error was found in relation to that solution. *Ode45*, *ode113*, and *ode23* were the most accurate solvers, but each solution took 30 to 60 seconds. The most accurate solver condition under 2 seconds was *ode15s* with a MaxStep=0.1 option. This option forces the largest iteration step to be less than 0.1 days. This solver condition was chosen for solving the model.

Table 3.1
Solution time and error of several solver conditions

Solver	Options	Solution Time (s)	Error
ode45		60.33	0
ode23		38.48	1.53×10^{-11}
ode113		54.20	3.14×10^{-11}
ode23t		0.36	1.45×10^{-06}
ode15s		0.40	5.88×10^{-07}
ode15s	MaxStep=0.5	0.39	3.81×10^{-07}
ode15s	MaxStep=0.1	0.42	9.27×10^{-08}
ode23s		1.66	4.84×10^{-07}
ode23s	MaxStep=0.5	1.67	2.03×10^{-07}
ode23s	MaxStep=0.1	1.91	1.98×10^{-07}
ode23tb		0.39	5.86×10^{-07}
ode23tb	MaxStep=0.5	0.39	2.21×10^{-07}
ode23tb	MaxStep=0.1	0.42	1.63×10^{-07}

3.1.3 Model Solution of Salubrinal and Loading Treatments

Solving the model under normal conditions with loading during weeks 5-8 resulted in a 0.4% increase in osteoblast activity and a 0.2% decrease in osteoclast activity that increased BMD by about 4.5% (Figure 3.2A). Salubrinal treatment did not change the model solution. Applying OVX to the model, osteoblasts holds steady while osteoclast activity increases about 4%, resulting in a 33% dip after 8 weeks (Figure 3.2B). Under loading, osteoblast activity increased 0.4%, osteoclast activity increased 4%, and BMD decreased only 30%, while under salubrinal application, osteoblast activity increased 0.3%, osteoclast increased 3%, and BMD decreased by only 27%. A year later (Figure 3.2C), BMD decrease plateaus at 46%. Salubrinal

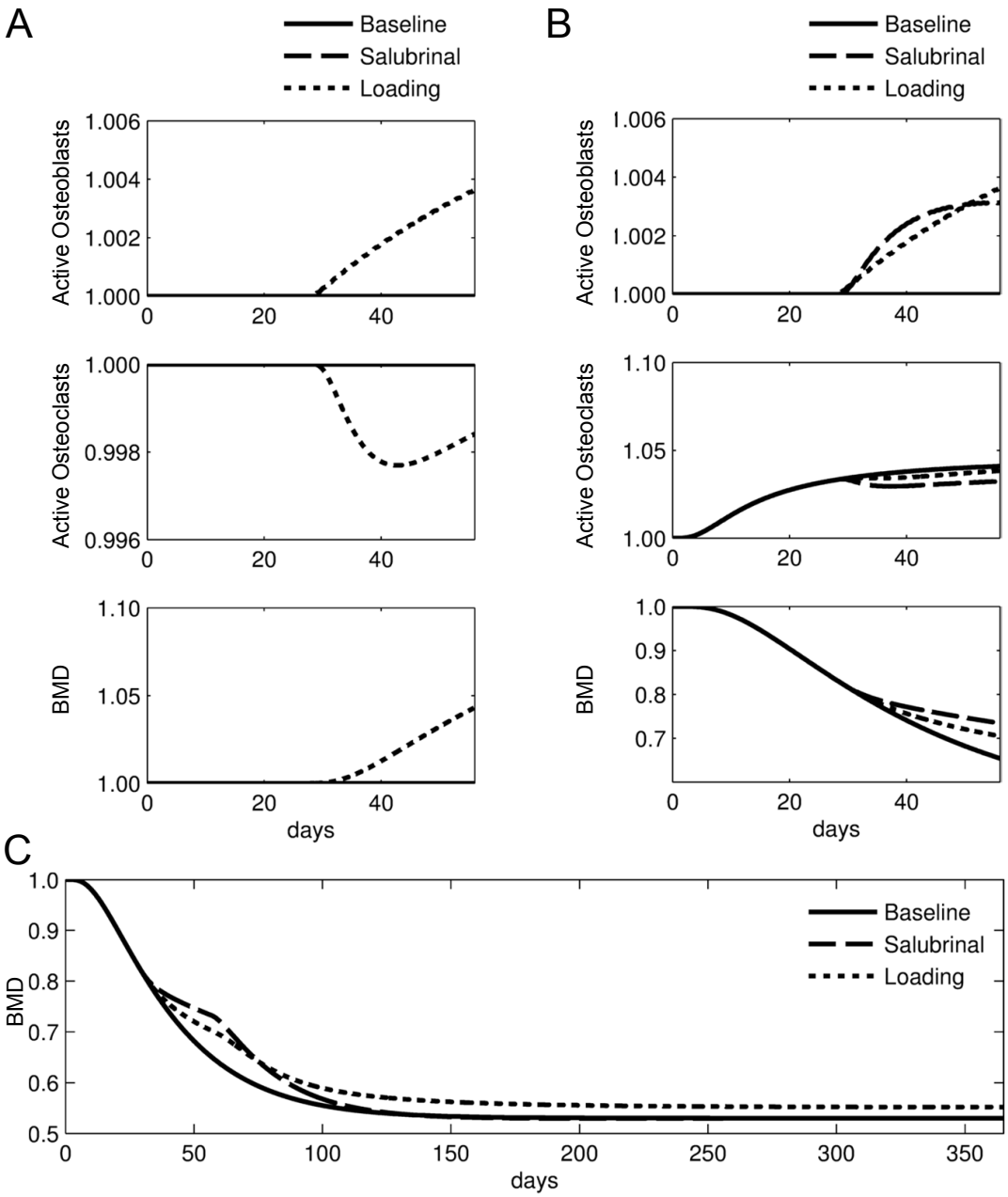

Fig. 3.2. Comparison of the model solutions for baseline (no treatment), salubrinal, and knee loading. (A) Effects of knee loading on normalized osteoblast number, normalized osteoclast number, and BMD to the normal mice. (B) Effects of knee loading and salubrinal on normalized osteoblast number, normalized osteoclast number, and BMD to the ovariectomized mice. OVX was applied on day 1 and treatment was applied weeks 5-8. (C) Long-term effects of BMD in response to 4-week treatment to the ovariectomized mice.

treatment quickly returns to the ovariectomy baseline after 8 more weeks, but loading maintains a slight bias, decreasing only 44%.

Figure 3.3 shows a trajectory of the osteoblasts and osteoclasts after OVX and with loading and salubrinal treatment. After OVX, the osteoclast number increases. After treatment intervention during weeks 5-8, osteoclast number increases while the increase in osteoclasts is mitigated.

3.1.4 Parameter Sensitivity of Model

Figures 3.4A and 3.4B show the sensitivity of the osteoclast-related parameters. The two rate constants for the formation and dissociation of the OPG-RANKL complex, k_{OL} and d_{OL}, trend in opposite directions. Increasing the formation constant k_{OL} increases the peak BMD from knee loading, while increasing the dissociation constant d_{OL} decreases peak BMD from knee loading. The rate constants of the RANK-RANKL complex similarly trend in opposing directions. Increasing the formation constant k_{KL} decreased the peak BMD from salubrinal treatment, while decreasing dissociation constant d_{KL} decreased the peak BMD from salubrinal treatment.

Osteoblast-related parameters behaved differently (Figure 3.4C-D). Increasing the sclerostin-dependence constant β_{SC} increased the effect of mechanical loading exponentially. The constant for p-eIF2α effect on ATF4, k_{APE}, increased the effect of salubrinal treatment as it increased.

3.1.5 Particle Swarm Parameter Sensitivity

Several different parameter values for velocity correction ratio α and global contribution ratio β were tried. Parameter values $\alpha = 1$ and $\beta = 1$ were found to work the best (Figure 3.5).

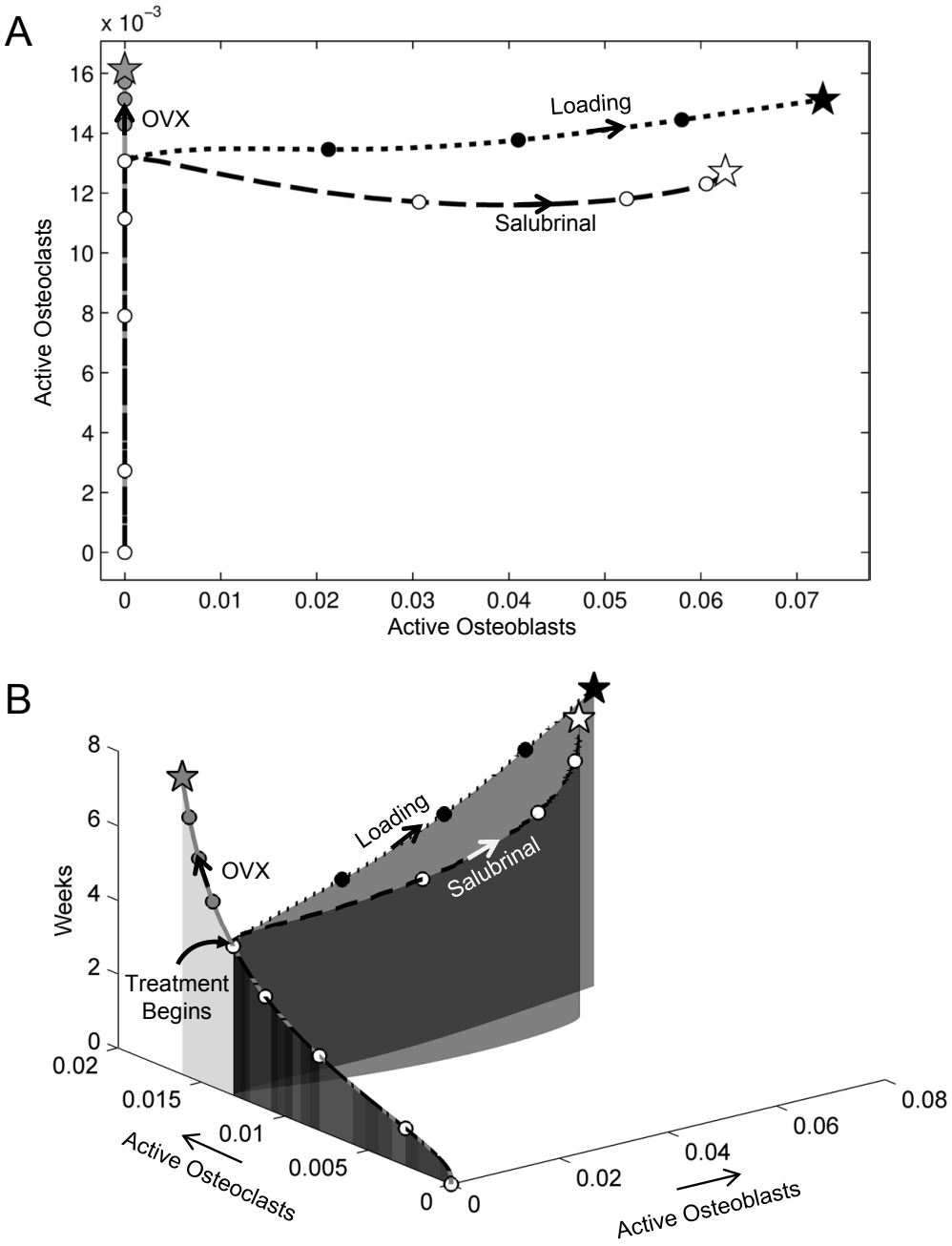

Fig. 3.3. Changes in the normalized numbers of osteoblasts and osteoclasts in response to knee loading and salubrinal on the ovariectomized mice. (A) Two-dimensional trajectory in the osteoblast-osteoclast plane. (B) Three-dimensional trajectory, in which the vertical axis denotes time. Each circle represents position after each week. Note that the grey, white, and black circles indicate no treatment (OVX), salubrinal, and knee loading, respectively.

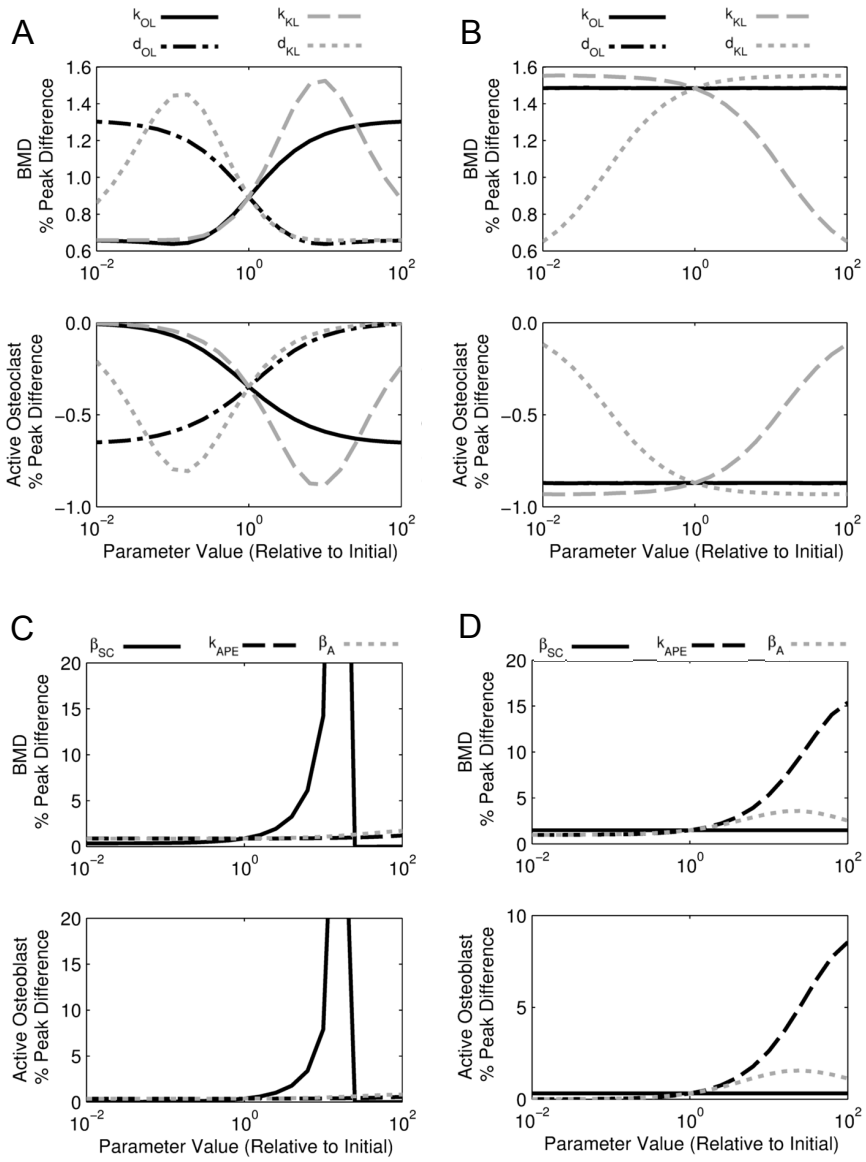

Fig. 3.4. Parameter sensitivity of the treatment in weeks 5-8. (A) Effects of the osteoclast-related parameters (k_{OL}, d_{OL}, k_{KL}, and d_{KL}) on BMD and the normalized osteoclast number in response to knee loading. (B) Effects of the osteoclast-related parameters on BMD and the normalized osteoclast number in response to salubrinal. (C) Effects of the osteoblast-related parameters (β_{SC}, k_{APE}, and β_A) on BMD and the normalized osteoblast number in response to knee loading. (D) Effects of the osteoblast-related parameters on BMD and the normalized osteoblast number in response to salubrinal.

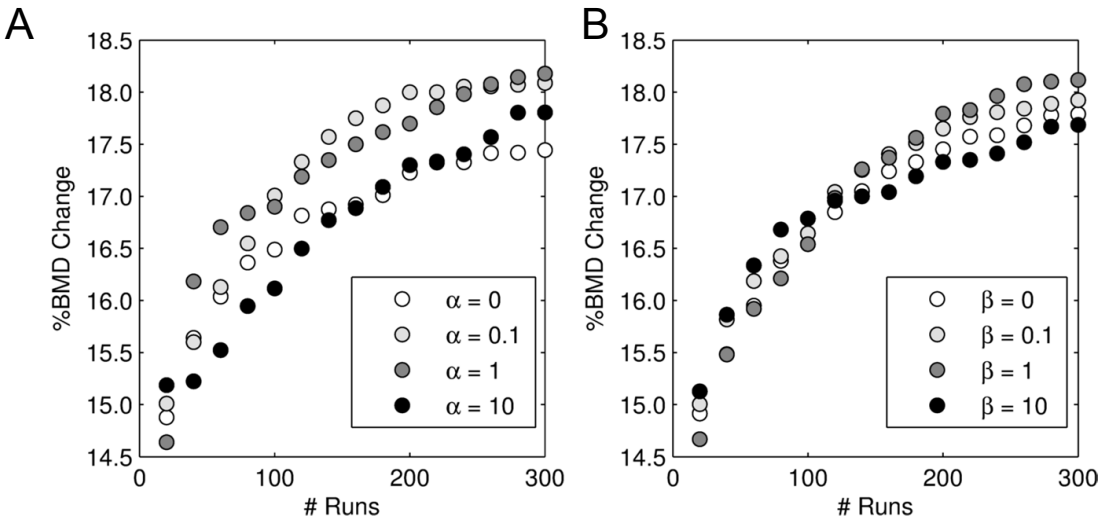

Fig. 3.5. Parameter sensitivity of the particle swarm search. The horizontal axis denotes the number of times the computational runs were conducted. (A) Effects of the velocity correction parameter α from 0 to 10 on the change in BMD. (B) Effects of the global contribution ratio β from 0 to 10 on the change in BMD.

3.1.6 Evaluation of Treatment Regimens

Figure 3.6A shows the best five treatment regimens found among all combinations of 8-week treatments. Three weeks of knee loading followed by 5 weeks of salubrinal injection was found to give the best BMD increase. Figure 3.6B shows the osteoblast, osteoclast, and BMD response to the baseline OVX, the best treatment, 8 weeks of salubrinal, and 8 weeks of loading. The initial bout of loading allows the optimal treatment case to work slightly better than the pure salubrinal case.

Figure 3.6C shows the best five treatment regimens found by particle swarm optimization. The best treatment was found to start with 10 weeks of loading followed by 6 weeks of salubrinal. Figure 3.6D shows the osteoblast, osteoclast, and BMD response in 16 weeks of baseline OVX, the top treatment, 16 weeks of salubrinal, and 16 weeks of loading. The best treatment regimen can be seen to follow the 16-week loading trajectory until week 11, when salubrinal is introduced.

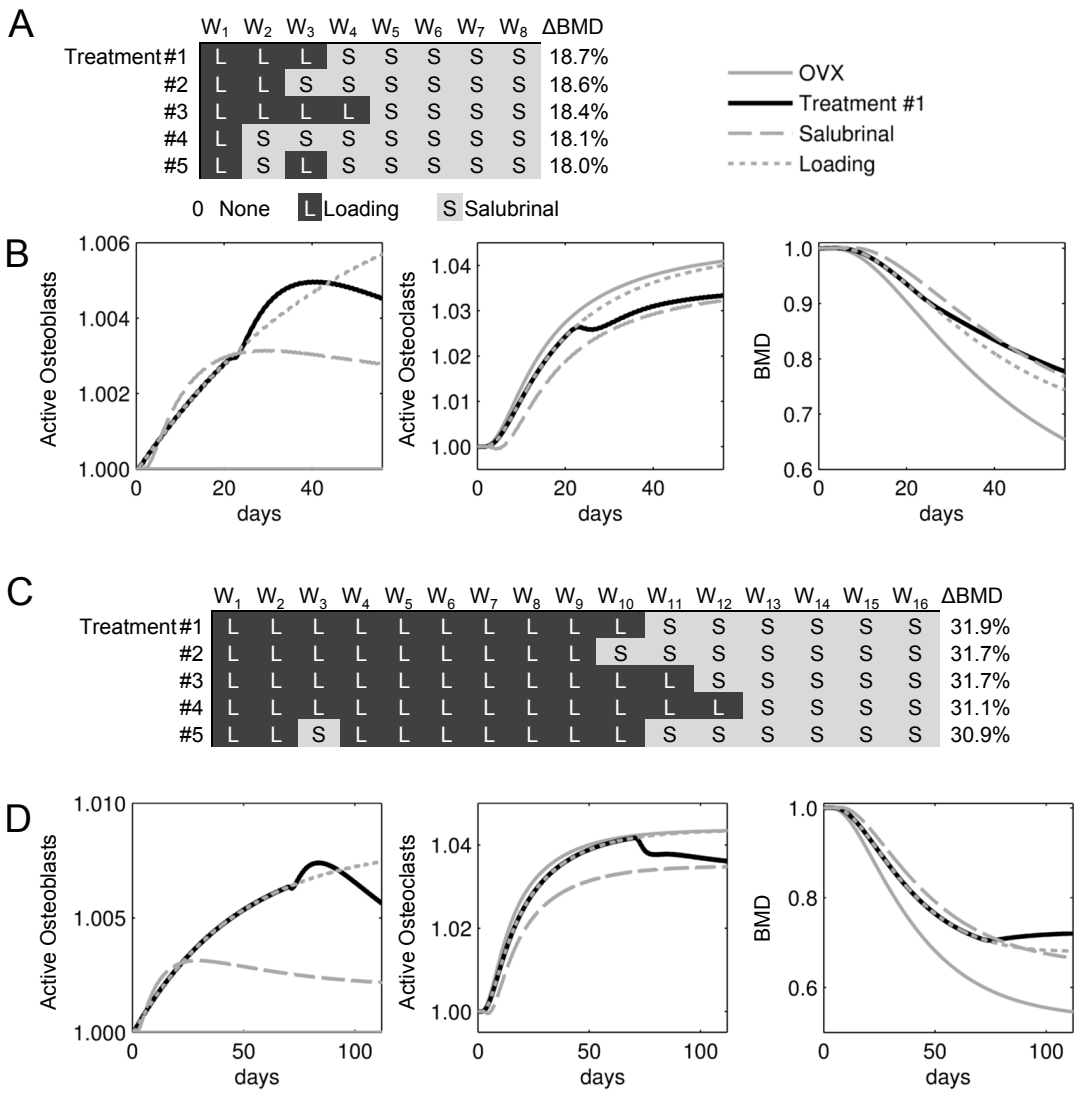

Fig. 3.6. Evaluation of treatment regimens by selecting knee loading or salubrinal on a weekly basis. (A & B) Top five 8-week treatment regimens from brute-force search. The changes in the normalized number of osteoblast and osteoclasts, and BMD in response to no treatment, treatment #1, salubrinal alone, and knee loading alone are shown. (C & D) Top five 16-week treatment regimens from particle swarm search. The changes in response to no treatment, treatment #1, salubrinal alone, and knee loading alone are shown.

3.1.7 Evaluating Treatment Costs

Figure 3.7A shows the optimal treatment regimen found by particle swarm for several values of k_{cost} and $\epsilon = 2$ (salubrinal is twice as costly as loading). When cost has no contribution, the treatment regimen begins with 17 weeks of loading followed by 7 weeks of salubrinal. As cost of treatment becomes increasingly prohibitive, the treatments move toward the point of data collection at the end, and salubrinal becomes scarce (Table 3.2). The response of osteoblast, osteoclast, and BMD to each treatment regimen is shown in Figure 3.7B. The delayed start of each successively restrictive k_{cost} parameter value can be seen in the delays of the osteoblast and osteoclast numbers. The BMD values of each cost parameter shoot off the baseline OVX case as treatment begins.

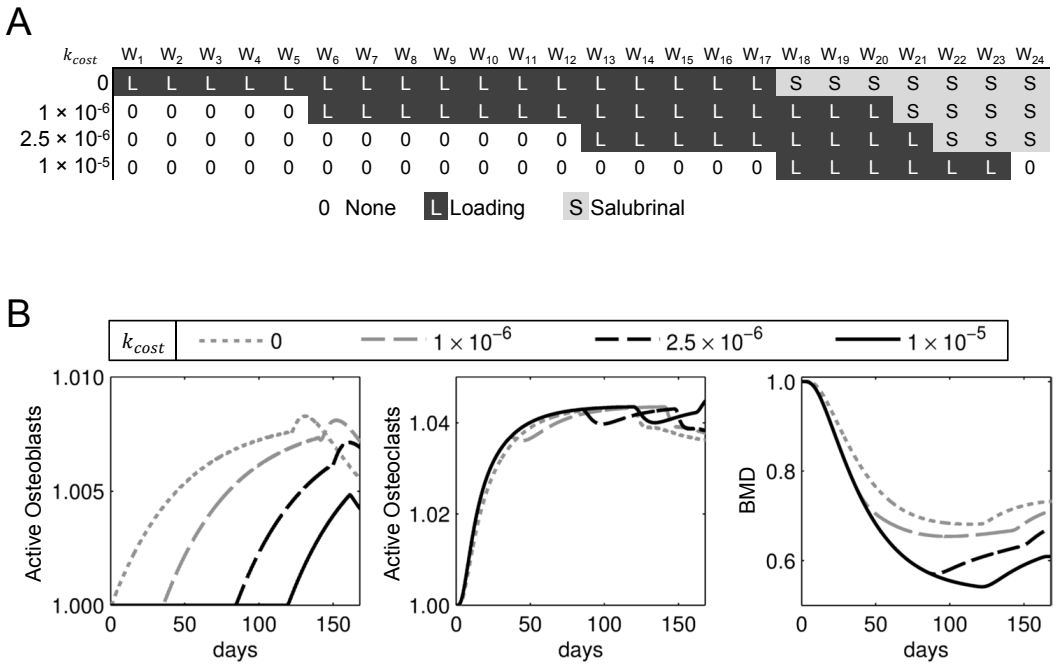

Fig. 3.7. Optimal treatment regimen considering treatment cost. (A) Top treatment regimen for each value of k_{cost} as found by particle swarm search. (B) Responses of normalized osteoblast, osteoclast, and BMD to each regimen as well as the baseline OVX condition.

Table 3.2
Change in BMD, cost, and fitness function J for best solution to values of k_{cost}

k_{cost}	ΔBMD	Cost	J
0	37.68%	0	0.0717
1×10^{-6}	33.75%	0.0259	0.1093
2.5×10^{-6}	26.66%	0.0276	0.1341
1×10^{-5}	14.49%	0.0176	0.1706

3.2 Osteoarthritis Model

To build a potential model for the regulation of ADAMTS5, first several RNA silencing experiments were performed. Quantitative PCR and Western blotting were performed to quantify the results of gene knockdown experiments. The gene expression microarray results of Lrp5 silencing were analyzed with a TFBM prediction algorithm, and several possible genes involved in transcriptional control were identified. From these, two potentially involved genes, IL1β and p-p38 MAPK, were identified, and their involvement was validated with RNA silencing. These results were collectively analyzed to create a network model of Lrp5 regulation of ADAMTS5 through IL1β and p-p38 MAPK, whose parameters were solved and characterized.

3.2.1 Lrp5, IL1β, and p38 MAPK Silencing Affect ADAMTS5

Both microarray and quantitative real-time PCR data revealed that the deletion of Lrp5 by RNA interference using two different sequences (Lrp5a and Lrp5b) elevated the level of ADAMTS5 mRNA (Figure 3.8). Western blot analysis revealed that both sequences of LRP5 siRNA elevated the phosphorylation of p38 MAPK (Figure 3.9A-B). Applying p38 siRNA decreased total and phosphorylated p38 MAPK, while a double knockdown with LRP5 siRNA showed a slight recovery in the phosphorylated p38 MAPK level (Figure 3.9C). ADAMTS5 mRNA levels decreased after p38 siRNA (Figure 3.9D). Double knockdown of both p38 siRNA and LRP5 siRNA slightly

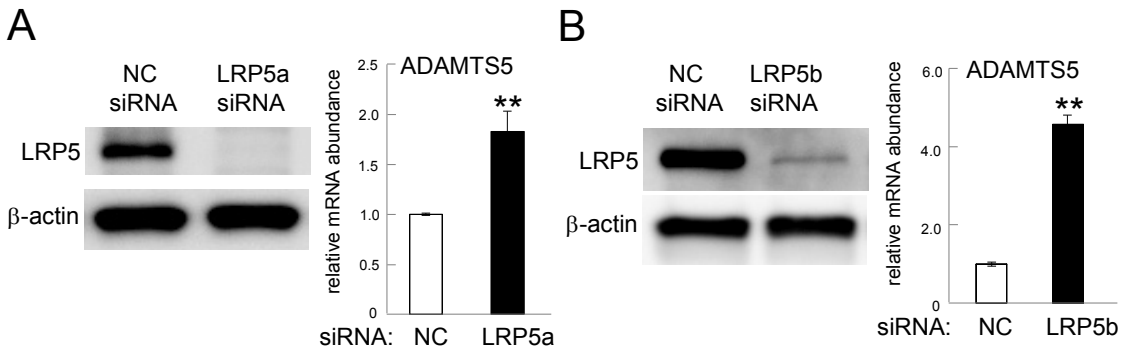

Fig. 3.8. Effects of LRP5 silencing. NC: non-specific siRNA. RNA interference using two LRP5 siRNAs and its effect on ADAMTS5 mRNA level.

decreases the elevation of ADAMTS5 mRNA caused by a single knockdown of just LRP5 siRNA.

IL1β is significantly silenced from a single knockdown with IL1β siRNA, while a double knockdown with both IL1β siRNA and LRP5 siRNA mitigated the IL1β mRNA elevation induced by a single knockdown with LRP5 siRNA (Figure 3.10A). Knockdown with only IL1β siRNA did not affect ADAMTS5 mRNA, but a double knockdown with IL1β siRNA and LRP5 siRNA decreased the ADAMTS5 mRNA increase observed in a single knockdown with LRP5 siRNA (Figure 3.10B).

3.2.2 TFBM prediction

The ant algorithm software predicted several potential TFBMs. The top predicted motifs included AAAGCC/GGCTTT, CGTAGC/GCTACG, CTTTTA/TAAAAG, and TAACCA/TGGTTA. Figure 3.11 shows the final pheromone level of each candidate motif, with the best ones labeled. These candidate motifs were located in the promoter sequence of a variety of genes, shown in Table 3.3. A general review of the literature involving these genes suggested a few potential genes and pathways that may be involved in ADAMTS5 regulation. The genes ATF2, MYC, FURIN, SERPINA1, and CEBPB were found to be related to Wnt signaling, p38 MAPK signaling,

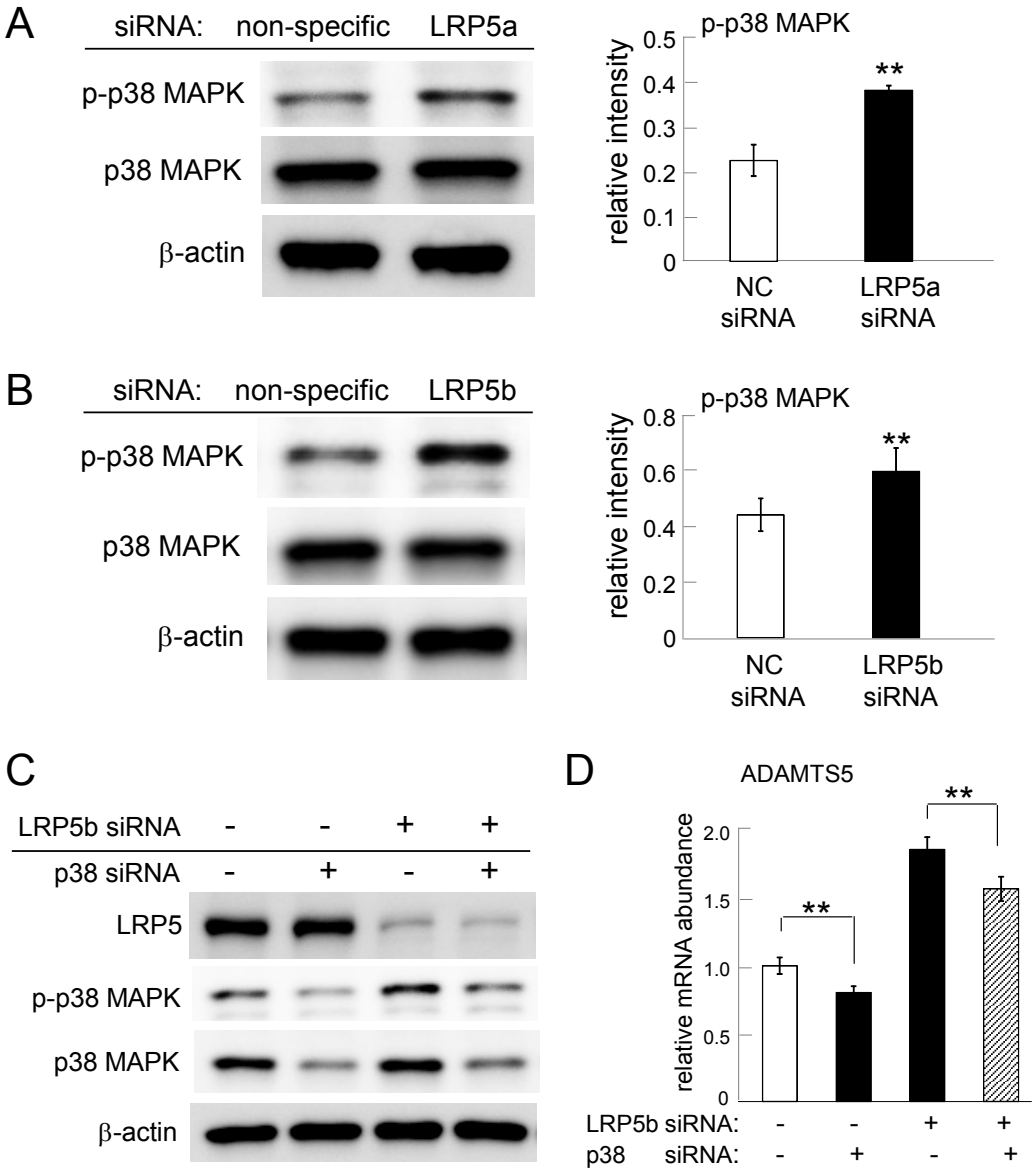

Fig. 3.9. Involvement of p38 MAPK in regulation of ADAMTS5 mRNA level in LRP5 silencing. Note that the double asterisk denotes $p < 0.01$. (A-B) Elevated phosphorylation level of p38 MAPK to LRP5 silencing using two LRP5 siRNAs. (C) Effect of double silencing of Lrp5 and p38 on Lrp5 and p38 MAPK phosphorylation. (D) Regulation of ADAMTS5 mRNA level in response to p38 siRNA and/or LRP5b siRNA.

IL1β, or ADAMTS5 by searching through the literature (Figure 3.12). The specific relationships are detailed further in the Discussion. From the filtered ($p < 0.05$)

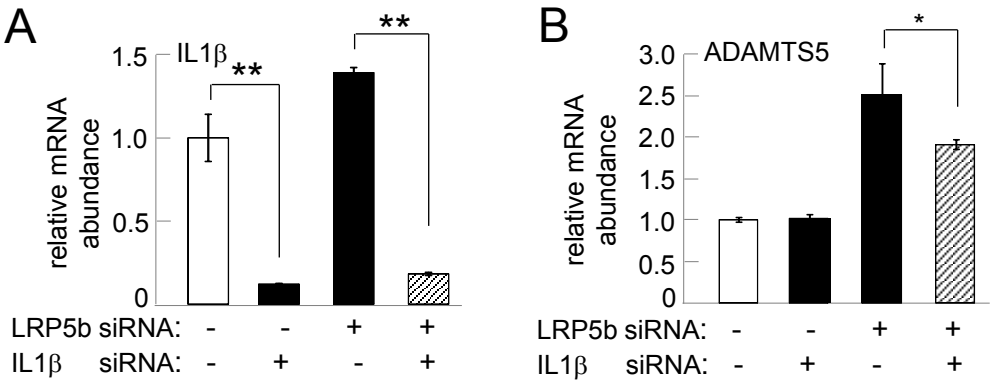

Fig. 3.10. Effects of LRP5 and IL1β silencing on the mRNA levels of ADAMTS5. Note that the double asterisk denotes $p < 0.01$, and "NC" denotes non-specific siRNA. (A) Levels of IL1β mRNA and (B) ADAMTS5 mRNA in response to LRP5 siRNA and/or IL1β siRNA.

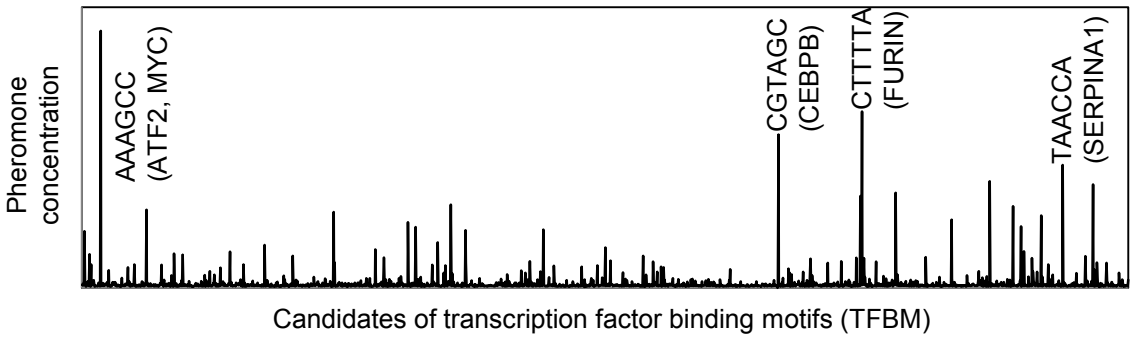

Fig. 3.11. Pheromone level of potential transcription factor binding motifs. Top 4 motifs are labeled with relevant genes.

microarray data, LRP5 and WNT3A were found to be downregulated, while MYC, CEBPB, IL1β, and ADAMTS5 were upregulated (Figure 3.13).

3.2.3 Regulatory Network Model

The results from the experiments led to a linear model of the pathway of LRP5, p38, and IL1β regulation of ADAMTS5 (Figure 3.14). The pathway depicts LRP5 inhibition of ADAMTS5, IL1β, and p38 MAPK. IL1β stimulation of LRP5's inhibition

Table 3.3
Genes whose promoter sequences contained the predicted motifs

Predicted Motif	Associated Gene	Transcription Factor	Promoter Sequence
AAAGCC	PCDHGB4	NFIC	GCTCTTGGCCCAAAGCCAGACCGG
	ATF2		ACACCGCCAAAGCCCTGC
	MYC	ENO1	AGGGTCGCGTGAGTATAAAAGCCGGTTTTCGGGG
	FGA	HNF1A	AGGACAAAGCCAAT
GGCTTT	POLA1	NFIC	cccgagccgctgATTGGCTttcagg
		CFY	
	RNU6-1	TBP	ggcTTTATATAtctt
	MMP1		ctGgctttct
	MT2A	MTF1	gggctttTGCACTCgtcccggctctt
	APOB		GAAATTCCTCTAGTCAGGTGGCTTTCTAATGGGTA CCCAGAGCCCTATGACTACCCAGATTGATGGTGCA CCCAACAGGAC
CTTTTA	ACTB	SRF	gTTCCGAaagttgCCTTTTATGG
		ELK4	
		ELK1	
	MYL3	SRF	CCTTTTATGG
	HBE1	NFY	aCCAATgacttttaagtacc
	ADH1B	CEBPA	CCTTTTATCTGTTTTGACAGTCTGGG
	FURIN	SP1	CACTTTTAGCTCCTCCCCCCA
	PDGFA		ccccctCCTTTTATGGagagag
TAAAAG	CD2		GATTAAAAGG
	MYC	ENO1	AGGGTCGCGTGAGTATAAAAGCCGGTTTTCGGGG
	HBG1		ataaaaGG
CGTAGC			
GCTACG	CEBPB		cgtgacgcagCGGTTGCTACGGGCCGCCCTtataaata
TAACCA	HBG1	NFY	ggccagccttgccttAACCAATagccttGACAAGgcaaactt
	LSP		TGCCAAACCCCAAAAACAaagaaccCTAACACCAgcctA ACCAGAT
TGGTTA	ALB	HNF1A	tGGTTAGtaattactaa
	SERPINA1		TGGTTAATATTCACCAgc
	COL1A1		GTGGTTAGC
	INS	PDX1	cccctggttaagacTCTAATGacccgctgg
	TCRA	ATF4	CCCATTTCCATGACGTCATGGTTA
	HMBS		tcAGTGTCCTGGttact
	PROC		agggccAAGCAAATATTTGTGGttatgga
	ANPEP	ZFHX3	TGGTTAATTTT

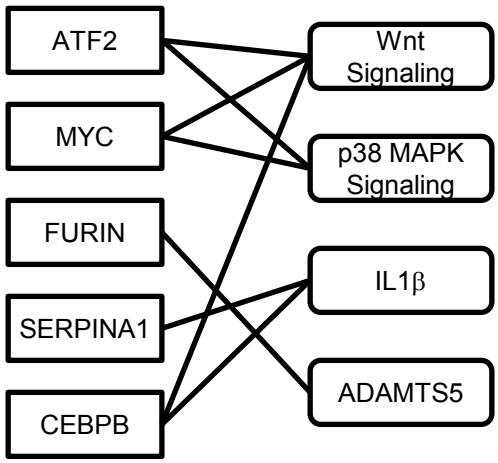

Fig. 3.12. Involvement of the targeted genes (ATF2, MYC, FURIN, SERPINA1, and CEBPB) in Wnt signaling, p38 MAPK signaling, IL1β, and ADAMTS5 from a literature search.

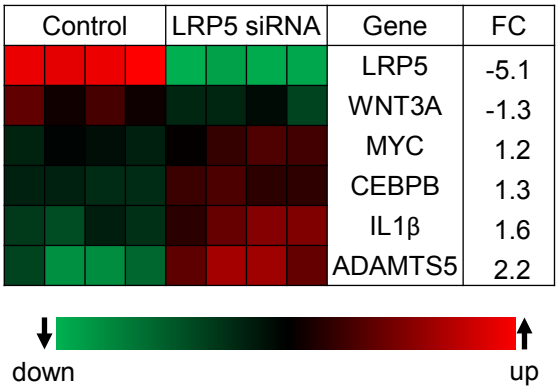

Fig. 3.13. Heat map of relevant genes from Lrp5 siRNA microarray data.

of ADAMTS5 as well as its own stimulation of ADAMTS5 and p38 are shown. Finally, p38 stimulates ADAMTS5, and an auxiliary stimulation of ADAMTS5, governed by parameter h, represents other regulatory factors not accounted for in the model.

Using experimental data (Table 3.4), the values of several parameters were estimated (Table 3.5). The parameters d, e, and h were explicitly determined, while the others (a, b, c, f, and g) were predicted as a hyperplane in parameter space. The allowable parameter values relating a, b, and c are depicted as a plane in three-

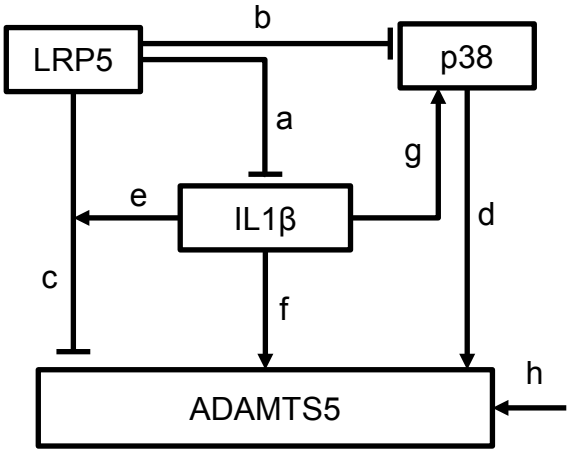

Fig. 3.14. Potential network model for LRP5, IL1β, and p38 MAPK regulation of ADAMTS5.

Table 3.4
Set of experimental data points

x_1	x_2	x_3	y	Remark
1	1	1	1	control
0	1	1	2.1	Lrp5 siRNA
1	0	1	1.05	IL1β siRNA
1	1	0	0.8	P38 siRNA
0	0	1	1.6	Lrp5 siRNA and IL1β siRNA
0	1	0	1.8	Lrp5 siRNA and p38 siRNA

dimensional space (Figure 3.15). Sample parameter values are also included as points on the plane.

Table 3.5
Regulatory Model Parameter Values

Parameter	Value
(a, b, c)	$0.05a + 0.3b + c \sim= 0.6$
d	~ 0.3
e	~ 0.45
(f, g)	$f + 0.3g \sim= 0.5$
h	~ 0.3

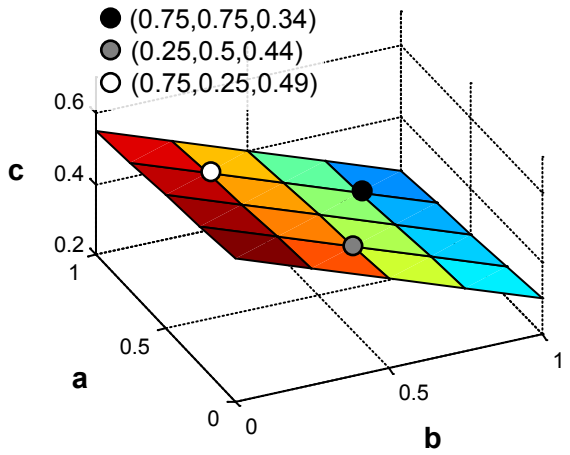

Fig. 3.15. Plane on which parameter values a, b, and c reside. The three dots mark sample parameter values.

4. DISCUSSION

The studies presented in this thesis illustrate how quantitative methods can be married with experimental data to increase their usefulness. These results may improve our understanding of pathways and potential intervention in the treatment of osteoporosis and osteoarthritis. Specifically, the quantitative analysis of a bone remodeling math model under administration of salubrinal and knee loading revealed a possible temporal difference between the two treatments. Quantitative analysis of Lrp5 regulation of ADAMTS5 suggested an expanded potential regulatory pathway to be investigated in treating osteoarthritis. Together, these analyses serve as examples of the promise of using quantitative methods to study new treatment methods.

4.1 Effectiveness of Salubrinal and Knee Loading in Osteoporosis Treatment

Salubrinal treatment and knee loading both improved the bone health of ovariectomized mice, as their bone mineral densities and osteoblast activities increased while their osteoclast activities decreased. The results demonstrate the promise of both salubrinal and knee loading in the treatment of post-menopausal osteoporosis, as both treatments reverse the negative effects of ovariectomy on the mice. Future studies may collect data at more time points to show the temporal character of the treatments.

4.2 Building a Mathematical Model of Bone Remodeling

The current model was based on work done previously [41]. While that model included the effects of the OPG/RANK/RANKL on precursor and active versions of both osteoblasts and osteoclasts, in order to simulate the experimental conditions, the

newer model includes the contributions of estrogen, sclerostin, p-eIF2α, ATF4, and NFATc1, as well as a variable for bone density. Estrogen was included to simulate the ovariectomized state, where after OVX, estrogen production decreased 75%. In the model, estrogen acts as an inhibitor of RANKL, as it has been found [45]. Sclerostin is an inhibitor of Wnt signaling and bone formation that is inhibited by mechanical loading [6]. Fluid flow-induced loading upregulates OPG [46], most likely by inhibiting sclerostin downregulation of OPG and upregulation of RANKL [47]. In the model sclerostin acts as an inhibitor of OPG.

Salubrinal acts by increasing the amount of phosphorylation of eIF2α. This elevation in phosphorylation has been shown to upregulate ATF4 [48] and downregulate NFATc1 expression [24]. However, mechanical loading has been shown to slightly suppress the phosphorylation of eIF2α [49]. This contradiction was modeled using a deadzone for p-eIF2α's effect, where loading's suppression of p-eIF2α did not propagate to ATF4 and NFATc1. The deadzone size was also estrogen-dependent, since salubrinal only affected the bone density of ovariectomized mice and not normal mice (data not shown). ATF4 was modeled to increase the differentiation rate of osteoblast precursors to active osteoblasts, while NFATc1 was modeled to increase the production of osteoclast precursors. Binding of RANKL to RANK induces osteoclast proliferation through NFATc1 [23], and the RANK-RANKL complex was modeled to stimulate NFATc1. Finally, the active osteoblasts and osteoclasts were modeled to increase and decrease, respectively, bone mineral density.

4.3 Assessing the Mathematical Model

Defining realistic parameters is an important step in building a useful math model. Though we tried to use existing literature to help define the parameter values, matching the model to the experimental results was the priority. Parameter sensitivity analysis (Figure 3.4) was used to identify which parameters could be adjusted and which direction they needed to go to better match the experimental results. Through

this process, however, parameter ratios that had a experimental counterpart were retained. Additionally, we wanted the long-term effects of our simulations to still be reasonable. For example, early iterations of parameter sets matched the experimental results at 8 weeks, but if the simulation time was extended to one year, the BMD would decrease into negative. Thus, parameter sets whose BMD equilibrium after OVX was reasonable were chosen.

Since BMD was the state variable that subsequent algorithms would use as a fitness function, its magnitude was more vigorously matched than osteoclast or osteoblast numbers. Additionally, the ALP and TRAP staining assays used to quantify osteoblasts and osteoclasts evalutate their relative activities, not necessarily their number. Thus, in adjusting parameters to match experimental data, the directional change in osteoblast and osteoclast numbers were settled for, and only BMD was numberically matched.

Choosing appropriate solver conditions is also valuable to ensure both an accurate result and a realistic computational time. For this, we tested a variety of solver algorithms and solving conditions. *Ode45* is the most commonly used solver for well-behaving systems. For this model, it took about a minute to solve 56 days. A brute force search of all 6,561 possible 8-week treatment regimens would take 4.5 days. The most accurate solver that took less than 2 seconds was *ode15s* with the 'MaxStep' option set to 0.1. At solving time of 0.42s, the brute force search would take only 45 minutes.

Expanding the brute force search to 16-week treatment regimens would require 43 million solutions. For a solving time 0.42s, that would take 209 days. Thus an optimization algorithm is required to find the best treatment regimen in a reasonable amount of time. Particle Swarm Optimization was chosen to find near-optimal solutions in less than 1000 iterations, or about 7 minutes.

4.4 Features of Predicted Treatment Regimens

The predictions from the described model revealed unobvious behavior of the model and suggested a few new treatment strategies to study. Loading was found to be more effective when applied earlier, as its effects are long term. Salubrinal seems to have a more immediate effect, thus being more advantageous when applied closer to the data collection time. Because of this timing mismatch, salubrinal and loading are not additive, and thus optimizing treatment scheduling is valuable. The mathematical model suggests that first applying loading then injecting salubrinal will improve the response in BMD over only loading or only salubrinal. It will be valuable and interesting to confirm this prediction *in vivo*. The best treatment regimens found by particle swarm optimization agreed with those found by a brute force search of all possible 8-week treatment regimens, confirming the usefulness of particle swarm as a predictive tool. Adding a cost consideration to the analysis showed how the model dealt with budgetary constraints. As the contribution of treatment cost increased, the treatments were pushed later to maximize the effect at the time of measurement.

4.5 Novel Features of Model

To more accurately represent the system dynamics, this model utilized a few novel features. Experimental data has shown that mechanical loading actually inhibits the phosphorylation of eIF2α, but it does not interfere with the NFATc1-mediated regulation of osteoclast activity by RANK-RANKL. Salubrinal was also found to be ineffective in increasing BMD in non-ovariectomized mice. These effects were controlled by an estrogen-dependent dead zone function. Within a certain range, small fluctuations in p-eIF2α did not change ATF4 and NFATc1. However, under the OVX condition, when estrogen decreased, the dead zone shrinks so that smaller changes to p-eIF2α affected ATF4 and NFATc1. A non-Markov bias on BMD was also applied after each bout of mechanical loading. Performing mechanical loading gradually increased the equilibrium of BMD, approximating experimental results [50].

4.6 Osteoporosis Model Limitations

This model and optimization method represent a first step in evaluating optimal treatment protocols, and there are a few limitations future iterations should address. Though many parameters are based on experimental values, some are crude estimates, adjusted to fit experimental results, which could affect both the timing and magnitude of the model's response to stimuli. Additional parameter validation might be needed for further accuracy. This model considered only a single value of BMD, but responses may differ depending on bone type and location of stimulus. Additionally, the dead zone and loading bias are mathematical approximations of complex interactions unable to be modeled through ordinary linear equations. Though these are necessary for the model's accuracy, a more sophisticated understanding of each mechanism may yield a better mathematical description.

4.7 Role of Lrp5, IL1β, and p38 MAPK in ADAMTS5 Regulation

Our silencing experiments show that Lrp5-mediated signaling is involved in reducing p38 MAPK signaling and interleukin responses. Silencing Lrp5 elevates the phosphorylation of p38 MAPK, and a double deletion with p38 siRNA and Lrp5 siRNA suppresses the upregulation of ADAMTS5 induced by Lrp5 siRNA. This suggests an intermediary role for p38 in Lrp5-mediated regulation of ADAMTS5. Similarly, a double deletion of IL1β and Lrp5 attenuates the increase in the level of ADAMTS5 mRNA caused by Lrp5 siRNA alone. However, unlike in p38 MAPK, where a deletion of p38 significantly decreased transcription of ADAMTS5, a single deletion of IL1β caused no significant change to ADAMTS5 mRNA level. This observation suggests that p38 MAPK and IL1β act differently in the Lrp5-mediated regulation of ADAMTS5.

4.8 Microarray Analysis

To further evaluate genome-wide and siRNA-based experimental results, we employed the ant algorithm to predict potential TFBMs. Based on these results, ATF2, MYC, FURIN, SERPINA1, and CEBPB were predicted to regulate transcription of ADAMTS5. These molecules are all reported to be linked to activation of p38 MAPK, Wnt signaling, ADAMTS5, and/or inflammatory and degenerative responses. In response to Wnt3a, for instance, ATF2 is activated via p38 MAPK in mouse and human embryonic cell lines [51]. Also, activation of MYC is mediated by p38 MAPK [52], and it is inhibited by Wnt signaling [53]. FURIN codes a protein that converts ADAMTS5 to its active form [54]. SERPINA1 is up-regulated in chondrocyte cells in response to IL1β stimulation [55], and CEBPB was reported to mediate IL1β-induced expression of collagenases such as MMP1 and MMP13 [56].

4.9 Regulatory Model of ADAMTS5

Based on the experimental results, a regulatory network model was developed in which the parameters representing interactions among Lrp5, IL1β, p38 MAPK, and ADAMTS5 were estimated using the results of siRNA-based experiments. The up-regulation of ADAMTS5 by Lrp5 knockdown suggests that Lrp5 inhibits ADAMTS5 expression. Lrp5 knockdown also increases the phosphorylation of p38 MAPK, suggesting an inhibitory role. Silencing p38 decreases ADAMTS5 expression both in single knockdown and double knockdown with Lrp5 siRNA, implying a stimulatory role of p-p38 on ADAMTS5. IL1β silencing does not change ADAMTS5 expression by itself; however, under double knockdown with Lrp5 siRNA, the expression of ADAMTS5 is reduced compared to the increased expression of single Lrp5 silencing. Lrp5 silencing also increases the expression of IL1β. This was modeled using a feedback loop between IL1β and Lrp5, where Lrp5 inhibits IL1β, and IL1β stimulates Lrp5's inhibition of ADAMTS5. Thus when IL1β is silenced, the lack of its direct

stimulation of ADAMTS5 is balanced by its lack of stimulation of Lrp5 inhibition. An additional stimulation from IL1β to p38 MAPK was added based on literature [57].

Each interaction in the model was labeled with a parameter, *a*-*h*. At first approximation, these parameters can be understood as the relative weights of each interaction. The results indicated that the components which are not directly linked to Lrp5, IL1β, or p38 MAPK, represented by h, also provide an effect on ADAMTS5 transcription. The combinational effect of IL1β directly on ADAMTS5 and through p38 (f and g) sums to 0.5, suggesting its efficacy is greater than those other components represented by h. The planar relation between the parameters representing Lrp5's effects on IL1β, p38 MAPK, and ADAMTS5 (a, b, and c, respectively) suggest a larger range of possible values of a and b than for c. For likely values of a and b, c will be close to f and d in value. Lrp5, however, still applies a large effect on the expression of ADAMTS5 through IL1β and p38 MAPK.

More experiments will be required to fully solve the parameters and to reveal other possible pathway features. The model can predict the results of possible experiments, and the actual results can be used to verify and update the model. Collectively, the results with siRNA-based experiments were quantitatively interpreted by the mathematical network model consistent with genome-wide expression data and the prediction of TFBMs with ant algorithm.

5. CONCLUSIONS

The work presented in this thesis demonstrates the potential of mathematical analysis in both finding new possible treatment actions and optimizing treatment outcomes. Using data gathered from experiments on a mouse model, a math model was created to simulate salubrinal and knee loading treatments. The regimen of these two treatments were optimized using Particle Swarm Optimization, and including cost in the analysis provided a first step toward using this analysis to factor in budgetary constraints when treating patients. Cell culture experiments were performed on chondrocytes to further elucidate the molecular action of osteoarthritis. A series of RNA interference experiments to silence Lrp5, p38 MAPK, and IL1β were performed, and the data collected was analyzed to predict genes possibly involved. This analysis lead to a math model of Lrp5 regulation on ADAMTS5.

Future studies can improve and extend the work done here. For the osteoporosis model, predicted treatments need to be validated using animal studies. These results can also inform how salubrinal and mechanical loading work together and help refine the pathways and parameters involved. More interventions can also be added to the model, such as bisphosphonates (through osteoclast impairment) or denosumab (through RANKL inhibition). Side effect management could also be modeled. For example, salubrinal has been found to inhibit cancer responses [58], while PTH therapy has been found to lead to osteosarcomas in rats [59]. Incorporating these oncological pathways could assess the possibility of using salubrinal to mitigate the cancer risk of PTH. Also, parameters could be matched to personalize an individual's response to each treatment. This would allow the model to head toward clinical application.

Molecular signaling of osteoarthritis is not fully understood, and this work can help attack this problem in a different way. Future analysis may include microarray analysis of several other silencing experiments, and the combined results could lead

to additional features of this pathway. The regulatory model may expand to include more molecular players and interactions.

LIST OF REFERENCES

LIST OF REFERENCES

[1] D. J. Hadjidakis and I. I. Androulakis, "Bone remodeling," *Annals of the New York Academy of Sciences*, vol. 1092, no. 1, pp. 385–396, 2006.

[2] P. Ducy, R. Zhang, V. Geoffroy, A. L. Ridall, and G. Karsenty, "Osf2/Cbfa1: A transcriptional activator of osteoblast differentiation," *Cell*, vol. 89, no. 5, pp. 747–754, 1997.

[3] X. Yang, K. Matsuda, P. Bialek, S. Jacquot, H. C. Masuoka, T. Schinke, L. Li, S. Brancorsini, P. Sassone-Corsi, T. M. Townes, A. Hanauer, and G. Karsenty, "ATF4 is a substrate of RSK2 and an essential regulator of osteoblast biology: Implication for coffin-lowry syndrome," *Cell*, vol. 117, no. 3, pp. 387–398, 2004.

[4] S. L. Teitelbaum, "Bone resorption by osteoclasts," *Science*, vol. 289, no. 5484, pp. 1504–1508, 2000.

[5] L. F. Bonewald, "The amazing osteocyte," *Journal of Bone and Mineral Research*, vol. 26, no. 2, pp. 229–238, 2011.

[6] A. G. Robling, P. J. Niziolek, L. A. Baldridge, K. W. Condon, M. R. Allen, I. Alam, S. M. Mantila, J. Gluhak-Heinrich, T. M. Bellido, S. E. Harris, and C. H. Turner, "Mechanical stimulation of bone in vivo reduces osteocyte expression of Sost/sclerostin," *Journal of Biological Chemistry*, vol. 283, no. 9, pp. 5866–5875, 2008.

[7] L. J. Raggatt and N. C. Partridge, "Cellular and molecular mechanisms of bone remodeling," *Journal of Biological Chemistry*, vol. 285, no. 33, pp. 25103–25108, 2010.

[8] T. Uzawa, M. Hori, S. Ejiri, and H. Ozawa, "Comparison of the effects of intermittent and continuous administration of human parathyroid hormone(1-34) on rat bone," *Bone*, vol. 16, no. 4, pp. 477–484, 1995.

[9] R. S. Weinstein, R. L. Jilka, A. M. Parfitt, and S. C. Manolagas, "Inhibition of osteoblastogenesis and promotion of apoptosis of osteoblasts and osteocytes by glucocorticoids. potential mechanisms of their deleterious effects on bone.," *Journal of Clinical Investigation*, vol. 102, no. 2, pp. 274–282, 1998.

[10] C. Christiansen, B. Riis, and P. Rodbro, "Prediction of rapid bone loss in postmenopausal women," *The Lancet*, vol. 329, no. 8542, pp. 1105–1108, 1987.

[11] L. A. Armas and R. R. Recker, "Pathophysiology of osteoporosis new mechanistic insights," *Endocrinology and metabolism clinics of North America*, vol. 41, no. 3, pp. 475–486, 2012.

[12] M. J. Favus, "Bisphosphonates for osteoporosis," *N. Engl. J. Med.*, vol. 363, no. 21, pp. 2027–2035, 2010.

[13] P. D. Delmas, "Clinical potential of RANKL inhibition for the management of postmenopausal osteoporosis and other metabolic bone diseases," *Journal of Clinical Densitometry*, vol. 11, no. 2, pp. 325–338, 2008.

[14] S. R. Cummings, J. S. Martin, M. R. McClung, E. S. Siris, R. Eastell, I. R. Reid, P. Delmas, H. B. Zoog, M. Austin, A. Wang, *et al.*, "Denosumab for prevention of fractures in postmenopausal women with osteoporosis," *N. Engl. J. Med.*, vol. 361, no. 8, pp. 756–765, 2009.

[15] J. Zanchetta, C. Bogado, J. Ferretti, O. Wang, M. Wilson, M. Sato, G. Gaich, G. Dalsky, and S. Myers, "Effects of teriparatide [recombinant human parathyroid hormone (1–34)] on cortical bone in postmenopausal women with osteoporosis," *Journal of Bone and Mineral Research*, vol. 18, no. 3, pp. 539–543, 2003.

[16] M. Edwards, S. Bain, M. Bailey, M. Lantry, and G. Howard, "17-beta estradiol stimulation of endosteal bone formation in the ovariectomized mouse: An animal model for the evaluation of bone-targeted estrogens," *Bone*, vol. 13, no. 1, pp. 29–34, 1992.

[17] G. P. Dalsky, K. S. Stocke, A. A. Ehsani, E. Slatopolsky, W. C. Lee, and S. C. Lee, "Weight-bearing training and lumbar bone mineral content in postmenopausal women.," *Ann. Intern. Med.*, vol. 108, no. 6, pp. 824–828, 1988.

[18] A. Simkin, J. Ayalon, and I. Leichter, "Increased trabecular bone density due to bone-loading exercises in postmenopausal osteoporotic women," *Calcified Tissue International*, vol. 40, no. 2, pp. 59–63, 1987.

[19] P. Zhang, S. M. Tanaka, H. Jiang, M. Su, and H. Yokota, "Diaphyseal bone formation in murine tibiae in response to knee loading," *Journal of Applied Physiology*, vol. 100, no. 5, pp. 1452–1459, 2006.

[20] D. Burr, A. Robling, and C. Turner, "Effects of biomechanical stress on bones in animals," *Bone*, vol. 30, no. 5, pp. 781–786, 2002.

[21] Y.-X. Qin, T. Kaplan, A. Saldanha, and C. Rubin, "Fluid pressure gradients, arising from oscillations in intramedullary pressure, is correlated with the formation of bone and inhibition of intracortical porosity," *Journal of Biomechanics*, vol. 36, no. 10, pp. 1427–1437, 2003. ¡ce:title¿Bone Cell and Tissue Mechanics¡/ce:title¿.

[22] M. Boyce, K. F. Bryant, C. Jousse, K. Long, H. P. Harding, D. Scheuner, R. J. Kaufman, D. Ma, D. M. Coen, D. Ron, and J. Yuan, "A selective inhibitor of eIF2α dephosphorylation protects cells from ER stress," *Science*, vol. 307, no. 5711, pp. 935–939, 2005.

[23] H. Takayanagi, S. Kim, T. Koga, H. Nishina, M. Isshiki, H. Yoshida, A. Saiura, M. Isobe, T. Yokochi, J. Inoue, E. F. Wagner, T. W. Mak, T. Kodama, and T. Taniguchi, "Induction and activation of the transcription factor NFATc1 (NFAT2) integrate RANKL signaling in terminal differentiation of osteoclasts," *Developmental Cell*, vol. 3, no. 6, pp. 889–901, 2002.

[24] K. Hamamura, N. Tanjung, and H. Yokota, "Suppression of osteoclastogenesis through phosphorylation of eukaryotic translation initiation factor 2 alpha," *J. Bone Miner. Metab.*, pp. 1–11, 2013.

[25] L. He, J. Lee, J. H. Jang, K. Sakchaisri, J. Hwang, H. J. Cha-Molstad, K. A. Kim, I. J. Ryoo, H. G. Lee, S. O. Kim, N. K. Soung, K. S. Lee, Y. T. Kwon, R. L. Erikson, J. S. Ahn, and B. Y. Kim, "Osteoporosis regulation by salubrinal through eIF2α mediated differentiation of osteoclast and osteoblast," *Cellular Signalling*, vol. 25, no. 2, pp. 552–560, 2013.

[26] H. Gray, P. Williams, and L. Bannister, *Gray's Anatomy: The Anatomical Basis of Medicine and Surgery*. Churchill Livingstone, 1995.

[27] M. B. Goldring, "The role of the chondrocyte in osteoarthritis," *Arthritis & Rheumatism*, vol. 43, no. 9, pp. 1916–1926, 2000.

[28] J. Bertrand, C. Cromme, D. Umlauf, S. Frank, and T. Pap, "Molecular mechanisms of cartilage remodelling in osteoarthritis," *The International Journal of Biochemistry & Cell Biology*, vol. 42, no. 10, pp. 1594–1601, 2010.

[29] R. F. Loeser, S. R. Goldring, C. R. Scanzello, and M. B. Goldring, "Osteoarthritis: A disease of the joint as an organ," *Arthritis & Rheumatism*, vol. 64, no. 6, pp. 1697–1707, 2012.

[30] H. Stanton, J. Melrose, C. B. Little, and A. J. Fosang, "Proteoglycan degradation by the ADAMTS family of proteinases," *Biochimica et Biophysica Acta (BBA) - Molecular Basis of Disease*, vol. 1812, no. 12, pp. 1616–1629, 2011.

[31] F. P. Luyten, P. Tylzanowski, and R. J. Lories, "Wnt signaling and osteoarthritis," *Bone*, vol. 44, no. 4, pp. 522–527, 2009.

[32] T. Yuasa, T. Otani, T. Koike, M. Iwamoto, and M. Enomoto-Iwamoto, "Wnt/β-catenin signaling stimulates matrix catabolic genes and activity in articular chondrocytes: its possible role in joint degeneration," *Laboratory Investigation*, vol. 88, no. 3, pp. 264–274, 2008.

[33] R. J. U. Lories, J. Peeters, A. Bakker, P. Tylzanowski, I. Derese, J. Schrooten, J. T. Thomas, and F. P. Luyten, "Articular cartilage and biomechanical properties of the long bones in Frzb-knockout mice," *Arthritis & Rheumatism*, vol. 56, no. 12, pp. 4095–4103, 2007.

[34] K. Sawakami, A. G. Robling, M. Ai, N. D. Pitner, D. Liu, S. J. Warden, J. Li, P. Maye, D. W. Rowe, R. L. Duncan, M. L. Warman, and C. H. Turner, "The Wnt co-receptor LRP5 is essential for skeletal mechanotransduction but not for the anabolic bone response to parathyroid hormone treatment," *Journal of Biological Chemistry*, vol. 281, no. 33, pp. 23698–23711, 2006.

[35] L. Lodewyckx, F. P. Luyten, and R. J. Lories, "Genetic deletion of low-density lipoprotein receptor-related protein 5 increases cartilage degradation in instability-induced osteoarthritis," *Rheumatology*, vol. 51, no. 11, pp. 1973–1978, 2012.

[36] I. Papathanasiou, K. N. Malizos, and A. Tsezou, "Low-density lipoprotein receptor-related protein 5 (LRP5) expression in human osteoarthritic chondrocytes," *Journal of Orthopaedic Research*, vol. 28, no. 3, pp. 348–353, 2010.

[37] L. Bianchi, M. Dorigo, L. M. Gambardella, and W. J. Gutjahr, "A survey on metaheuristics for stochastic combinatorial optimization," *Natural Computing: an international journal*, vol. 8, no. 2, pp. 239–287, 2009.

[38] J. Kennedy and R. C. Eberhart, "A discrete binary version of the particle swarm algorithm," in *Systems, Man, and Cybernetics, 1997. Computational Cybernetics and Simulation., 1997 IEEE International Conference on*, vol. 5, pp. 4104–4108, IEEE, 1997.

[39] Y. Liu and H. Yokota, "Artificial ants deposit pheromone to search for regulatory DNA elements," *BMC Genomics*, vol. 7, no. 1, p. 221, 2006.

[40] M. Dorigo and G. Di Caro, "Ant colony optimization: a new meta-heuristic," in *Evolutionary Computation, 1999. CEC 99. Proceedings of the 1999 Congress on*, vol. 2, IEEE, 1999.

[41] A. Chen, K. Hamamura, P. Zhang, Y. Chen, and H. Yokota, "Systems analysis of bone remodelling as a homeostatic regulator," *IET Systems Biology*, vol. 4, pp. 52–63, Jan. 2010.

[42] Y. Liu and H. Yokota, "Modeling transcriptional regulation in chondrogenesis using particle swarm optimization," in *Computational Intelligence in Bioinformatics and Computational Biology, 2005. CIBCB '05. Proceedings of the 2005 IEEE Symposium on*, pp. 1–7, 2005.

[43] A. B. Chen, K. Hamamura, G. Wang, W. Xing, S. Mohan, H. Yokota, and Y. Liu, "Model-based comparative prediction of transcription-factor binding motifs in anabolic responses in bone," *Genomics, Proteomics & Bioinformatics*, vol. 5, no. 3, pp. 158–165, 2007.

[44] V. Matys, E. Fricke, R. Geffers, E. Gössling, M. Haubrock, R. Hehl, K. Hornischer, D. Karas, A. E. Kel, O. V. Kel-Margoulis, D.-U. Kloos, S. Land, B. Lewicki-Potapov, H. Michael, R. Münch, I. Reuter, S. Rotert, H. Saxel, M. Scheer, S. Thiele, and E. Wingender, "TRANSFAC: transcriptional regulation, from patterns to profiles," *Nucleic Acids Research*, vol. 31, no. 1, pp. 374–378, 2003.

[45] S. Bord, D. Ireland, S. Beavan, and J. Compston, "The effects of estrogen on osteoprotegerin, RANKL, and estrogen receptor expression in human osteoblasts," *Bone*, vol. 32, no. 2, pp. 136–141, 2003.

[46] C. H. Kim, L. You, C. E. Yellowley, and C. R. Jacobs, "Oscillatory fluid flow-induced shear stress decreases osteoclastogenesis through RANKL and OPG signaling," *Bone*, vol. 39, no. 5, pp. 1043–1047, 2006.

[47] A. R. Wijenayaka, M. Kogawa, H. P. Lim, L. F. Bonewald, D. M. Findlay, and G. J. Atkins, "Sclerostin stimulates osteocyte support of osteoclast activity by a RANKL-dependent pathway," *PLoS One*, vol. 6, no. 10, p. e25900, 2011.

[48] K. Hamamura and H. Yokota, "Stress to endoplasmic reticulum of mouse osteoblasts induces apoptosis and transcriptional activation for bone remodeling," *FEBS Letters*, vol. 581, no. 9, pp. 1769–1774, 2007.

[49] P. Zhang, C. Jiang, E. Ledet, and H. Yokota, "Loading- and unloading-driven regulation of phosphorylation of eIF2α," *Biological Sciences in Space*, vol. 25, no. 1, pp. 3–6, 2011.

[50] S. J. Warden, R. K. Fuchs, A. B. Castillo, I. R. Nelson, and C. H. Turner, "Exercise when young provides lifelong benefits to bone structure and strength," *Journal of Bone and Mineral Research*, vol. 22, no. 2, pp. 251–259, 2007.

[51] R. K. Bikkavilli, M. E. Feigin, and C. C. Malbon, "p38 mitogen-activated protein kinase regulates canonical Wnt–β–catenin signaling by inactivation of GSKβ," *Journal of Cell Science*, vol. 121, no. 21, pp. 3598–3607, 2008.

[52] M. J. Kim, B.-J. Park, Y.-S. Kang, H. J. Kim, J.-H. Park, J. W. Kang, S. W. Lee, J. M. Han, H.-W. Lee, and S. Kim, "Downregulation of FUSE-binding protein and c-myc by tRNA synthetase cofactor p38 is required for lung cell differentiation," *Nature genetics*, vol. 34, no. 3, pp. 330–336, 2003.

[53] Z. You, D. Saims, S. Chen, Z. Zhang, D. C. Guttridge, K.-l. Guan, O. A. MacDougald, A. M. Brown, G. Evan, J. Kitajewski, and C.-Y. Wang, "Wnt signaling promotes oncogenic transformation by inhibiting c-Myc-induced apoptosis," *J. Cell Biol.*, vol. 157, no. 3, pp. 429–440, 2002.

[54] J.-M. Longpré, D. R. McCulloch, B.-H. Koo, J. P. Alexander, S. S. Apte, and R. Leduc, "Characterization of proADAMTS5 processing by proprotein convertases," *The International Journal of Biochemistry & Cell Biology*, vol. 41, no. 5, pp. 1116–1126, 2009.

[55] B. Ma, C. A. van Blitterswijk, and M. Karperien, "A Wnt–β–catenin negative feedback loop inhibits interleukin-1β-induced matrix metalloproteinase expression in human articular chondrocytes," *Arthritis & Rheumatism*, vol. 64, no. 8, pp. 2589–2600, 2012.

[56] B. L. Petrella, D. A. Armstrong, and M. P. Vincenti, "CCAAT-enhancer-binding protein beta activation of MMP-1 gene expression in SW1353 cells: Independent roles of extracellular signal-regulated and p90/ribosomal S6 kinases," *Journal of Cellular Physiology*, vol. 226, no. 12, pp. 3349–3354, 2011.

[57] J. A. Mengshol, M. P. Vincenti, C. I. Coon, A. Barchowsky, and C. E. Brinckerhoff, "Interleukin-1 induction of collagenase 3 (matrix metalloproteinase 13) gene expression in chondrocytes requires p38, c-jun N-terminal kinase, and nuclear factor κB: Differential regulation of collagenase 1 and collagenase 3," *Arthritis & Rheumatism*, vol. 43, no. 4, pp. 801–811, 2000.

[58] M. Koizumi, N. G. Tanjung, A. Chen, J. R. Dynlacht, J. Garrett, Y. Yoshioka, K. Ogawa, T. Teshima, and H. Yokota, "Administration of salubrinal enhances radiation-induced cell death of SW1353 chondrosarcoma cells," *Anticancer Research*, vol. 32, no. 9, pp. 3667–3673, 2012.

[59] J. L. Vahle, G. G. Long, G. Sandusky, M. Westmore, Y. L. Ma, and M. Sato, "Bone neoplasms in F344 rats given teriparatide [rhpth(1-34)] are dependent on duration of treatment and dose," *Toxicologic Pathology*, vol. 32, no. 4, pp. 426–438, 2004.

APPENDICES

A. EQUATIONS FOR BONE REMODELING MATH MODEL

A.1 Differential Equation Definitions

In addition to the OPG/RANK/RANKL pathway interaction with osteoblasts and osteoclasts defined previously, four molecular players, estrogen, sclerostin, ATF4, and NFATc1, were included with BMD in an expanded mathematical model of bone remodeling:

$$\dot{x}_O(t) = p_O - d_O x_O(t) - \dot{x}_{OL}(t) - k_{OSC} x_{SC}(t) \tag{A.1}$$

$$\dot{x}_L(t) = p_L - d_L x_L(t) - \dot{x}_{OL}(t) - \dot{x}_{KL}(t) - k_E x_E(t) \tag{A.2}$$

$$\dot{x}_{OL}(t) = k_{OL} x_O(t) x_L(t) - d_{OL} x_{OL}(t) \tag{A.3}$$

$$\dot{x}_{KL}(t) = k_{KL} x_K(t) x_L(t) - d_{KL} x_{KL}(t) \tag{A.4}$$

$$\dot{N}_{pOB}(t) = \alpha_{pOB} - \beta_{SC} x_{SC}(t) - (\gamma_{pOB} + \alpha_{aOB}) N_{pOB}(t) \tag{A.5}$$

$$\dot{N}_{aOB}(t) = (\alpha_{aOB} + \beta_A x_A(t)) N_{pOB}(t) - \gamma_{aOB} N_{aOB}(t) \tag{A.6}$$

$$\dot{N}_{pOC}(t) = \alpha_{pOC} + \beta_N x_N(t) - (\gamma_{pOC} + \alpha_{aOC}) N_{pOC}(t) \tag{A.7}$$

$$\dot{N}_{aOC}(t) = \alpha_{aOC} N_{pOC}(t) - \gamma_{aOC} N_{aOC} \tag{A.8}$$

$$\dot{B}(t) = s_{OB} N_{aOB}(t) - s_{OC} N_{aOC}(t) - d_B B(t) + k_{Bmax} B_{max}(t) \tag{A.9}$$

$$\dot{x}_{SC}(t) = p_{SC} - d_{SC} x_{SC}(t) \tag{A.10}$$

$$\dot{x}_E(t) = p_E - d_E x_E(t) \tag{A.11}$$

$$\dot{x}_{PE}(t) = p_{PE} - d_{PE} x_{PE}(t) \tag{A.12}$$

$$\dot{x}_A(t) = p_A - d_A x_A(t) + k_{APE} \tilde{x}_{PE}(t) \tag{A.13}$$

$$\dot{x}_N(t) = p_N - d_N x_N(t) - k_{NPE} x_{PE}(t) + k_{NKL} x_{KL}(t) \tag{A.14}$$

$$\tilde{x}_{PE}(t) = \begin{cases} x_{PE}(t) - 0.8\frac{x_E(t)}{x_E^{REF}}x_{PE}^{REF} & \text{if } x_{PE}(t) \geq \left(1 + 0.8\frac{x_E(t)}{x_E^{REF}}\right)x_{PE}^{REF} \\ x_{PE}(t) + 0.8\frac{x_E(t)}{x_E^{REF}}x_{PE}^{REF} & \text{if } x_{PE}(t) \leq \left(1 - 0.8\frac{x_E(t)}{x_E^{REF}}\right)x_{PE}^{REF} \\ x_{PE}^{REF} & \text{otherwise} \end{cases} \tag{A.15}$$

$$B_{max}(t) = 1 - e^{-\lambda_{Bmax}(\Sigma N_{load})} \tag{A.16}$$

(A.17)

where $\dot{x}$ is the time derivative of state variable x, k is a rate constant, p is a synthesis rate, d is a degradation rate, α is a cell synthesis rate, β is a molecular interaction rate, and γ is a degradation rate. $\tilde{x}_{PE}(t)$ is a dead zone function introduced to account for the low sensitivity to salubrinal in healthy individuals. B_{max} accounts for bias for bone building caused by mechanical loading. The bias grows as the number of loading bouts increases. Specific definitions and values are found in Table 2.2.

A.2 Simulation of Experimental Conditions

The osteoporotic condition was simulated by decreasing the production by 75%:

$$p_E = \frac{p_E}{\tanh\left(5(t-1)\right) + 2} \tag{A.18}$$

Loading was simulated using a pulsed decrease in the production of sclerostin and phosphorylated eIF2α

$$p_{SC} = p_{SC} - p_{SC}\left(0.55e^{-50(mod(t,1)-0.5)^2}\right) \tag{A.19}$$

$$p_{PE} = p_{PE} - p_{PE}\left(0.5e^{-100(mod(t,1)-0.5)^2}\right) \tag{A.20}$$

(A.21)

Salubrinal treatment was simulated by a pulsed increase in the phosphorylation of eIF2α

$$p_{PE} = p_{PE} + p_{PE}\left(2.4e^{-100(mod(t,1)-0.5)^2}\right) \tag{A.22}$$

(A.23)

A.3 Reference Value Definitions

Reference values of the state variables (Table 2.3) were derived analytically:

$$x_O^{REF} = \frac{p_O - k_{OSC} x_{SC}^{REF}}{d_O} \tag{A.24}$$

$$x_L^{REF} = \frac{p_L - k_E x_E^{REF}}{d_L} \tag{A.25}$$

$$x_{OL}^{REF} = \left(\frac{k_{OL}}{d_{OL}}\right) x_O^{REF} x_L^{REF} \tag{A.26}$$

$$x_{KL}^{REF} = \left(\frac{k_{KL}}{d_{OL}}\right) x_L^{REF} x_K \tag{A.27}$$

$$N_{pOB}^{REF} = \frac{\alpha_{pOB} - \beta_{SC} x_{SC}^{REF}}{\gamma_{pOB} + \alpha_{aOB} + \beta_A x_A^{REF}} \tag{A.28}$$

$$N_{aOB}^{REF} = \left(\frac{\alpha_{aOB} + \beta_A x_A^{REF}}{\gamma_{aOB}}\right) N_{pOB}^{REF} \tag{A.29}$$

$$N_{pOC}^{REF} = \frac{\alpha_{pOC} + \beta_N x_N^{REF}}{\gamma_{pOC} + \alpha_{aOC}} \tag{A.30}$$

$$N_{aOC}^{REF} = \frac{\alpha_{aOC}}{\gamma_{aOC}} N_{pOC}^{REF} \tag{A.31}$$

$$B^{REF}(t) = \frac{s_{OB} N_{aOB}^{REF} - s_{OC} N_{aOC}^{REF}}{d_B} \tag{A.32}$$

$$x_{SC}^{REF} = \frac{p_{SC}}{d_{SC}} \tag{A.33}$$

$$x_E^{REF} = \frac{p_E}{d_E} \tag{A.34}$$

$$x_{PE}^{REF} = \frac{p_{PE}}{d_{PE}} \tag{A.35}$$

$$x_A^{REF} = \frac{p_A + k_{APE} x_{PE}^{REF}}{d_A} \tag{A.36}$$

$$x_N^{REF} = \frac{p_N - k_{NPE} x_{PE}^{REF} + k_{NKL} x_{KL}^{REF}}{d_N} \tag{A.37}$$

B. MATLAB SOURCE CODE

B.1 Model Function

```
function dX = dBoneAnt(t,X,regimen) % inputs: time, state
    variables, treatment regimen

dX = zeros(14,1); % initialize differential variable
% use globally defined parameters
global pO dO pL dL kOL dOL kKL dKL kKOC;
global apOB cpOB aaOB caOB apOC cpOC aaOC caOC bSC;
global sOB sOC dBMD;
global pSC dSC pE dE kLE kOSC pPE dPE pA dA pN dN kAPE kNPE kNKL
    bA bN;

xK = 1; % RANK = 1
% p_XX is perturbation of parameter value XX
p_pE = pE;
p_pO = pO;
p_pSC = pSC;
p_pPE  = pPE;

p_pE = pE/(tanh(5*(t-1))+3);  % induce OVX (estrogen decreased by
    3/4)

% Define Treatment Perturbations
if t < (length(regimen)),
```

```
  modt = mod(t,1);  % treatments applied daily
  switch regimen(floor(t)+1)  % choose which treatment to apply
    case 1 %sal
      p_pPE = pPE + pPE*(2.4*exp(-100*(modt-.5)^2));
    case 2 %load
      p_pSC = pSC-pSC*(.55*exp(-50*(modt-.5)^2));
      p_pPE = pPE-pPE*(.5*exp(-100*(modt-.5)^2));
    case 3 %sal + load
      p_pSC = pSC-pSC*(.55*exp(-50*(modt-.5)^2));
      p_pPE = pPE-pPE*(.5*exp(-100*(modt-.5)^2)) + pPE*(2.4*exp
          (-100*(modt-.5)^2));
  end
end

% perturbation of OB/OC parameters by new state variables
p_aaOB = aaOB + bA*X(13);
p_apOB = apOB - bSC*X(10);
p_apOC = apOC + bN*X(14);

% differential equations defined
dX(3) = kOL*X(1)*X(2) - dOL*X(3); %xOL
dX(4) = kKL*xK*X(2) - dKL*X(4); %xKL
dX(1) = p_pO - dO*X(1) - dX(3) - kOSC*X(10); %xO
dX(2) = pL - dL*X(2) - dX(3) - dX(4) - kLE*X(11); %xL
dX(5) = p_apOB - (cpOB+p_aaOB)*X(5); %NpOB
dX(6) = p_aaOB*X(5) - caOB*X(6) ; %NaOB
dX(7) = p_apOC - (cpOC+aaOC)*X(7); %NpOC
dX(8) = aaOC*X(7) - caOC*X(8); %NaOC

% BMD Bias
kbMax = 3e-6;
```

```
lbMax = 1e-2;
regend = floor(t)+1;
if regend > numel(regimen),
   regend = numel(regimen);
   BMDmax = kbMax*(1-exp(-lbMax*(sum(regimen(1:regend)>=2))));
else
   BMDmax = kbMax*(1-exp(-lbMax*(mod(t,1)*(regimen(regend)>=2)+sum
       (regimen(1:regend-1)>=2))));
end

dX(9) = sOB*X(6) - sOC*X(8) - dBMD*X(9) + BMDmax; %BMD
dX(10) = p_pSC - dSC*X(10); %xSC
dX(11) = p_pE - dE*X(11); %xE
dX(12) = p_pPE - dPE*X(12); %xPE

% p-eIF2a deadzone
delPE = 0.8*X(11)/pE*dE;
if X(12) >= (1+delPE)*pPE/dPE,
   zPE = X(12)-delPE*pPE/dPE;
elseif X(12) <= (1-delPE)*pPE/dPE,
   zPE = X(12)+delPE*pPE/dPE;
else
   zPE = pPE/dPE;
end

dX(13) = pA - dA*X(13) + kAPE*zPE; %xA
dX(14) = pN - dN*X(14) - kNPE*zPE + kNKL*X(4); %xN
```

B.2 Particle Swarm Optimization of Treatment

```
parameters; % initialize model parameters
```

```
tspan = [0 112];
wkno = 16;
opts = odeset('MaxStep',.1);
[tOVX,XOVX] = ode15s(@(t,X) dBoneAnt(t,X,0),tspan,X0,opts); % OVX
    case solution
% pso paramters
trials = 10;
alpha = 1;
eps = 1;
particles = 20;
omega = 1;
enditer = 5;
bestlog = zeros(1,trials); %bestval runs
logruns = zeros(1,trials);
bestreglog = zeros(trials,wkno); %best regimens found
for tr = 1:trials,
  p = rand(particles,wkno,3);
  pbest = zeros(particles,wkno,3);
  pbestval = zeros(particles,1);
  gbest = zeros(1,wkno,3);
  gbestval = 0;
  vel = zeros(particles,wkno,3);
  v0 = vel;
  gsame = 0;
  iters = 0;
  runs = 0;
  regimen = zeros(wkno,1);
  while gsame < enditer,
    iters = iters+1;
    gsame = gsame+1;
    for i = 1:particles,
```

```
for j = 1:size(p,2),
  p(i,j,:) = (p(i,j,:)/max(p(i,j,:)));
end
randnos = rand(wkno,1);
totalprob = sum(p(i,:,:),3);
for k = 1:wkno,
  if randnos(k) < p(i,k,1)/totalprob(k),
    regimen(k) = 0;
  elseif randnos(k) < sum(p(i,k,1:2))/totalprob(k),
    regimen(k) = 1;
  else
    regimen(k) = 2;
  end
  regW((1+7*(k-1)):(7*k)) = regimen(k);
end
[t,X] = ode15s(@(t,X) dBoneAnt(t,X,regW),tspan,X0,opts);
Cred = (X(end,9)-XOVX(end,9))/XOVX(end,9);
runs = runs + 1;
if pbestval(i) < Cred,
  pbestval(i) = Cred;
  pbest(i,:,:) = p(i,:,:);
end
if gbestval < Cred,
  gbestval = Cred;
  gbest = zeros(1,wkno,3);
  for k = 1:wkno,
    gbest(1,k,regimen(k)+1) = 1;
  end
  gsame = 0;
  disp([iters,i]);
end
```

```
    end
    rg = diag(rand(wkno,1));
    rp = diag(rand(wkno,1));
    for i = 1:particles,
      vel(i,:,:) = omega*v0(i,:,:) + reshape(alpha*(rg*squeeze(
          gbest-p(i,:,:))+eps*rp*squeeze(pbest(i,:,:)-p(i,:,:)))
          ,1,wkno,3);
      p(i,:,:) = p(i,:,:) + vel(i,:,:);
    end
    v0 = vel;
  end
  bestlog(tr) = gbestval;
  logruns(tr) = runs;
  [rmax,imax] = max(gbest,[],3);
  bestreglog(tr,:) = imax-1;
end
```